

Gravitational collapse of a volcano edifice as a trigger for explosive carbonatite eruption?

Vladislav Rapprich^{1,†}, Benjamin F. Walter^{2,3}, Veronika Kopačková-Strnadová¹, Tobias Kluge^{2,3}, Bohuslava Čejková¹, Ondřej Pour¹, John M. Hora¹, Jindřich Kynický⁴, and Tomáš Magna¹

¹Czech Geological Survey, Klárov 3, CZ-11821 Prague, Czech Republic

²Chair of Economic Geology and Geochemistry, Karlsruhe Institute of Technology, Adenauerring 20b, D-76131 Karlsruhe, Germany

³Laboratory for Environmental and Raw Material Analyses (LERA), Adenauerring 20b, D-76131 Karlsruhe, Germany

⁴BIC Brno, Ltd., Purkyňova 648/125, CZ-62100 Brno, Czech Republic

ABSTRACT

The Miocene Kaiserstuhl volcanic complex in the Rhine graben rift is known for simultaneously exposing both intrusive and erupted (pyroclastic) calciocarbonatites. This makes Kaiserstuhl a promising candidate for studying the field and genetic relations between intrusive calciocarbonatite and its eruptive equivalent, and the processes enabling eruption of the calciocarbonatite at the surface in particular. Eruptive calciocarbonatites in Kaiserstuhl are represented by carbonatite tuff and lapillistone beds covering a debrite fan on the western flank of the volcano. The debrites are interpreted as lahar (debris flow) and possibly also debris-avalanche deposits. Based on the observed textures, the debris flows were most likely derived by water dilution from debris avalanches resulting from edifice failure, which occurred in the central part of the Kaiserstuhl volcanic complex. The edifice failure ultimately exposed the intrusive system, and the carbonatite pyroclasts (lapilli and ash) were ejected from narrow vents represented by open-framework tuff-breccias aligned along the detachment scarp. Since the Ca-carbonates break down rapidly at high temperatures and low pressures, calciocarbonatites are unlikely to form surface lavas. On the other hand, the presence of the calciocarbonatite pyroclastic deposits suggests that some geological process faster than the high-temperature breakdown of Ca-carbonate may facilitate calciocarbonatite eruption. We suggest that the sudden ex-

posure and decompression of a suprasolidus high-level carbonatite intrusion by edifice collapse may be a suitable scenario enabling calciocarbonatite eruption. The absence of edifice failures on alkaline volcanoes, where carbonatite intrusion is either supposed or exposed, may explain the overall scarcity of erupted calciocarbonatites.

1. INTRODUCTION


Carbonatites are magmatic rocks with >50 modal % primary igneous carbonates and <20 wt% SiO₂, present mostly as intrusive bodies, with extrusive forms representing <10% of occurrences (Woolley and Church, 2005). Their ages span from the late Archean (Tupertalik, ca. 3.0 Ga; Bizzarro et al., 2002) to the present day (Oldoinyo Lengai, ca. 0.37 Ma to recent; Macintyre et al., 1974). Most carbonatite bodies worldwide are represented by calciocarbonatites, i.e., carbonatites with >80 wt% CaO from cation oxides (e.g., Woolley and Kempe, 1989). According to recent experimental studies, calciocarbonatites are most likely cumulate rocks crystallized from melts that may have had <50 wt% CaCO₃ (e.g., Weidendorfer et al., 2017). The predominantly intrusive nature of calciocarbonatites is also supported by experimental and inclusion-focused studies (Yaxley et al., 2022).

Our knowledge of the physical properties and eruptive behavior of carbonatite melts is still limited and mainly comes from the Oldoinyo Lengai volcano, a single carbonatite occurrence that, however, has a highly unusual sodic character (Dawson et al., 1990; Keller et al., 2010; Kervyn et al., 2010). The natrocarbonatite eruptions at Oldoinyo Lengai alternate with nephelinitic events. The extrusive natrocarbonatite activity

is mostly characterized by low eruption energy (volcanic explosivity index [VEI] = 0–1), whereas the nephelinitic events tend to be more powerful (VEI = 3), usually destroying the spectacular landforms of the preceding natrocarbonatite phase. The extremely low viscosity and rapid chilling at Oldoinyo Lengai create lava forms that are not seen at any other volcano.

Since modern human experience with carbonatite eruptions is limited to natrocarbonatite events at the Oldoinyo Lengai volcano, the experimental and petrogenetic research has also mainly focused on natrocarbonatites (e.g., Weidendorfer et al., 2017; Guzmics et al., 2019; Vasyukova et al., 2023), which are less sensitive to decompression and more prone to form carbonatite lavas than calcic carbonatites. The number of documented calciocarbonatite pyroclastic occurrences (Woolley and Church, 2005) implies that calciocarbonatite may also erupt at the surface under certain conditions—and this process requires better understanding as it has so far remained beyond the scope of modern studies.

The major problem for surface eruptions of carbonatite melts is the instability of calcium carbonate at high temperatures and low pressures that are typical of igneous rocks erupted at Earth's surface (see Shatskiy et al., 2013, and references therein), resulting in the swift breakdown to CaO and CO₂. This reaction is rapid at temperatures above 790 °C, but it becomes more sluggish at 600–790 °C (e.g., Karunadasa et al., 2019). The lower temperature limit for the magma mobility and eruption is given by the solidus temperature, determined by Podborodnikov et al. (2018) for CaCO₃ to exceed 800 °C at near-surface pressure conditions. This stability limit of CaCO₃ largely precludes formation of calciocarbonatite lavas, as the ascent and emplacement

Vladislav Rapprich  <https://orcid.org/0000-0003-4349-2116>

[†]vladislav.rapprich@geology.cz

ment rates are much slower than the breakdown reaction. On the other hand, explosive eruptions under favorable conditions may be fast enough to preserve primary magmatic CaCO_3 . The eruptive behavior of calciocarbonatite is an integral part of the evolution of high-level carbonatite complexes. Nevertheless, limited attention has been paid to the origin (from the perspective of physical volcanology) of calciocarbonatite pyroclastic rocks, except for reports describing their occurrence and mostly providing only basic textural observations, eventually focusing on their mineralogy or magmatic petrology (e.g., Kaiserstuhl, Germany—Keller, 1981; Barker, 2007; Rangwa, Kenya—Rosatelli et al., 2003; Ambinsky volcano, Primorye, Russia—Popov et al., 2007; Fort Portal, Uganda—Barker, 2007; Kerimasi, Tanzania—Reguir et al., 2008; Brava Island, Cape Verde—Mourão et al., 2010; Catanda, Angola—Campeny et al., 2014). Woolley and Church (2005) provided a comprehensive list of 53 extrusive carbonatite localities, but some of these occurrences remain to some extent speculative. Although calcite-dominated pyroclastic deposits documented on at least some volcanoes may be calcified natrocarbonatites (e.g., Deans and Roberts, 1984), and this aspect also requires specific attention, many other occurrences display primary calciocarbonatite textures.

To reveal the nature of volcanic processes leading to the eruption of calciocarbonatites, we focused on the Miocene Kaiserstuhl volcanic complex (herein referred to simply as Kaiserstuhl) in the Upper Rhine graben, Germany. This is one of the best-preserved volcanic systems where eruptive calciocarbonatites are present (Woolley and Church, 2005; Walter et al., 2018, 2020; Giebel et al., 2019). In addition, at Kaiserstuhl, subvolcanic feeding conduits and intrusive (carbonatite and silicate) facies are exposed (Wimmenauer and Schreiner, 2003; Braunger et al., 2018), which rarely is the case for younger volcanoes. Therefore, Kaiserstuhl appears to be an appealing candidate to delineate new ties to calciocarbonatite eruptions.

2. GEOLOGICAL SETTING

The Miocene (18–15 Ma) Kaiserstuhl volcanic complex in SW Germany is situated close to the eastern boundary of the Upper Rhine graben rift and is a part of the Central European magmatic province (Fig. 1A; e.g., Wilson and Downes, 2006; Lustrino and Wilson, 2007). The complex is structurally positioned at the junction of four major tectonic blocks within the rift and is affected by Neogene strike-slip and horst-graben tectonics within the rift (Beccaletto et al., 2010; Giebel et al., 2019). Generally gently dipping slopes, disturbed locally by erosional

cuestas, and a volcanic edifice composed mainly of lavas classify Kaiserstuhl as a shield volcano (Fig. 1B). The Kaiserstuhl volcanic complex consists mainly of mafic alkaline lavas intercalated with pyroclastic (mostly scoriae) beds, intruded by sills, alkaline dike rocks (alkaline lamprophyres and other alkaline rocks), and carbonatites (Fig. 1C). Extrusive carbonatites in the form of pyroclastic deposits occur on the western margin of Kaiserstuhl.

Erosion has exposed the polyphase subvolcanic center comprising various intrusive bodies and a rich variety of rock types (e.g., Wimmenauer and Schreiner, 2003, and references therein), for the purpose of this study merged into a single intrusive facies (Fig. 1C). The volcanic center is transected by numerous polygenetic diatreme breccias (e.g., Baranyi, 1971; Sigmund and Keller, 1994; Sigmund, 1996), which provided ascent pathways for several larger intrusive carbonatite bodies (Fig. 1C). The breccia matrix is composed of olivine melilitite (Sigmund, 1996). The sequence is further intruded by phonolite dikes and medium- to coarse-grained nosean syenite (e.g., Braunger et al., 2018; Giebel et al., 2019).

Based on the geochemistry and isotopic studies, the Kaiserstuhl silicate alkaline rocks have been interpreted to represent two distinct magma series: (1) “sodic” series (olivine nephelinites, hauyne melilitites, and melilitite hauynites) derived from a primitive ultrabasic melt and (2) “sodic-potassic” series (tephrites, phonolites, and syenites) that display a larger extent of fractionation (e.g., Schleicher et al., 1990; Wimmenauer and Schreiner, 2003; Braunger et al., 2018). According to Schleicher et al. (1990), Kaiserstuhl carbonatites are genetically linked to the “sodic” series. However, the detailed petrogenetic processes of the formation of carbonatites remain debated (e.g., Wang et al., 2014; Braunger et al., 2018; Walter et al., 2018, 2020, 2021).

At present, Quaternary colluvial, river, and eolian sediments (loess) cover most of the volcanic exposures. In addition, some parts have been significantly modified by anthropogenic land transformation related to viticulture. Despite limited exposure, the Kaiserstuhl volcanic complex is a classical site for petrological and geochemical studies due to its excellent accessibility, wide spectrum of rock types distributed over a small area, and association of carbonatites, alkaline rocks, and postmagmatic mineralization (e.g., Katz and Keller, 1981; Keller, 1981; Schleicher et al., 1990; Wang et al., 2014; Walter et al., 2018; Giebel et al., 2019; Ghobadi et al., 2022). On the other hand, both the geomorphology and physical volcanology have not been studied in detail.

3. METHODS

3.1. Volcanology and Volcanic Morphology

Since the genetic interpretations of volcanoclastic facies according to their textures (McPhie et al., 1993) are the key to our understanding of the eruptive history of any volcano, this study primarily focused on the volcanoclastic deposits to reconstruct the volcanic evolution and to better understand the mechanisms leading to explosive carbonatite eruptions. All available exposures of volcanoclastic rocks were systematically investigated and critically reinterpreted during two field campaigns in 2019 and 2021. The spatial and temporal (stratigraphic) relations of various volcanic facies were supported by morphological interpretations conducted using a light detection and ranging (LiDAR)-based digital elevation model (DEM) provided at 5 m spatial resolution by the Landesamt für Geo-information und Landentwicklung of Baden-Württemberg (LGL). The 5 m DEM was hydrologically corrected using the Topo to Raster tool provided in ArcGIS Desktop version 10.6.1. This procedure automatically removes spurious sinks or pits while maintaining stable, artifact-free behavior of the fitted surface grid (Sharma and Tiwari, 2014). Common DEM derivatives (slope, aspect, and shaded relief) were computed using the Spatial Analyst extension for ArcGIS with the aim to better visualize morphological features of the volcano.

3.2. Mineral Chemistry and Backscattered Electron Imaging

Quantitative chemical analyses of individual mineral phases and distribution maps of selected elements were obtained using a Tescan MIRA 3GMU electron microprobe analyzer (EMPA), housed at the laboratories of the Czech Geological Survey, Prague (CGS), fitted with a silicon drift detector (SDD) X-Max 80 mm² energy dispersive spectrometer (EDS) detector and driven by AZtecEnergy software (Oxford Instruments, Abingdon, UK). The analyses were acquired using 15 kV accelerating voltage, 15 mm working distance, 3 nA probe current, 30 s acquisition time, and 30 nm beam diameter. A mineral set of standards (SPI) and pure Co were used for standardization and beam calibration, respectively.

3.3. Stable C and O Isotopes and Clumped Isotopes

With an aim to verify the primary (magmatic) origin of the carbonatite lapilli in the studied pyroclastic deposits, the lapilli and secondary cement were analyzed for stable isotope com-

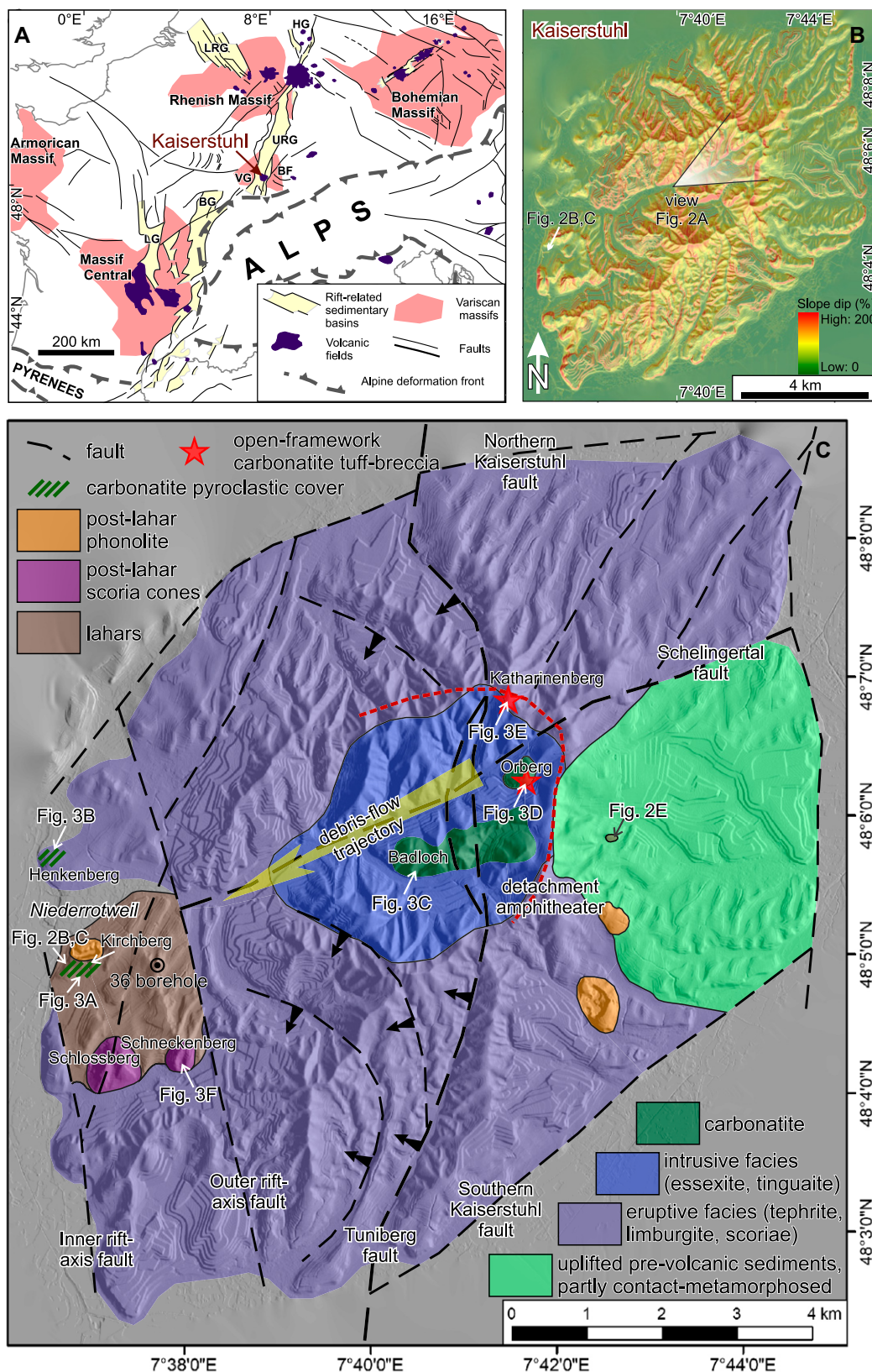


Figure 1. Geology of the Kaiserstuhl volcanic complex: (A) position of the Kaiserstuhl volcanic complex in the European Cenozoic rift system (adapted after Dèzes et al., 2004); (B) slope-dip analysis of the Kaiserstuhl volcanic complex based on light detection and ranging (LiDAR) data (source: Landesamt für Geoinformation und Landentwicklung of Baden-Württemberg [Baden-Württemberg State Office of Geoinformation and Land-development]); and (C) simplified geological map of the Kaiserstuhl (adapted after Wimmerauer and Schreiner, 2003; field observations and mapping [this study]). BF—Black Forest; BG—Bresse graben; HG—Hessian graben; LG—Limagne graben; LRG—Lower Rhine graben; URG—Upper Rhine graben; VG—Vosges.

positions of carbon and oxygen. The lapilli and cement fractions were separated manually using a small drill at the CGS. The conventional

stable C and O isotope compositions were determined following the decomposition procedure of McCrea (1950) and using a Thermo Scien-

tific™ Delta V Advantage isotope ratio mass spectrometer housed at the CGS. The results are reported in conventional delta (δ) notation

relative to Vienna standard mean ocean water (VSMOW) for oxygen and Vienna Pee Dee belemnite (VPDB) for carbon.

For selected samples, clumped isotope systematics ($^{16}\text{O}^{13}\text{C}^{18}\text{O}$; expressed as Δ_{638}) were determined using a TILDAS-FD-L2 laser spectroscopy system (Aerodyne Research Inc., Billerica, Massachusetts). Carbonate samples of ~ 12 mg mass were digested at 90 °C, and the resulting gas was processed as described in Weise and Kluge (2020). Measurement and data evaluation followed the principles described by Yanay et al. (2022). Isotopic calibration was based on the Inter-Carb approach (Bernasconi et al., 2021) and used the Δ_{47} -temperature calibration of Anderson et al. (2021).

3.4. Radiogenic Sr Isotopes

Strontium separation by column chromatography and isotope analyses using a Triton Plus thermal ionization mass spectrometer (TIMS; Thermo Fisher Scientific, Bremen, Germany) were done at the Czech Geological Survey. Powdered samples, either in the form of bulk samples or drilled domains within a sample, were dissolved in 4 mL of doubly distilled 2 M HCl, from which aliquots, corresponding to an estimated 500–1000 ng of Sr, were dried down and re-dissolved in HNO_3 , prior to further processing via column chromatography. Strontium was isolated from the dissolved matrix following an abbreviated version of the techniques described elsewhere (Pin et al., 1994; Míková and Denková, 2007) and using Sr resin (TrisKem International, Bruz, France).

Strontium isolated by column chromatography was loaded onto previously outgassed Ta single filaments that were allowed to develop an oxide coat. TIMS analyses were done in static mode, with simultaneous collection of ^{84}Sr , ^{85}Rb , ^{86}Sr , ^{87}Sr , and ^{88}Sr , at typical ion beam intensities of 5–7 V on mass ^{88}Sr for 100 ratios, each with 8 s integration time. Signal intensities were first corrected for gain and baseline, and the ^{87}Sr signal was corrected for isobaric interference using the measured ^{85}Rb signal and assuming $^{87}\text{Rb}/^{85}\text{Rb} = 0.386$. Isotopic ratios were corrected for instrumental mass fractionation assuming $^{86}\text{Sr}/^{88}\text{Sr} = 0.1194$. External reproducibility was estimated from repeated analyses over a 3 yr period of the Sr standard NBS-987 ($^{87}\text{Sr}/^{86}\text{Sr} = 0.710267 \pm 22$, 2σ ; $n = 87$).

4. RESULTS

4.1. Field Observations and Petrography

The landscape of Kaiserstuhl is dominated by remnants of structural slopes fragmented by

gullies (Fig. 1B), suggesting an early stage of erosion of the volcano. This contrasts with the landscape of eroded volcanic complexes dominated by high-level intrusive bodies (phonolite laccoliths) exposed by selective erosion (e.g., Raška and Cajz, 2016). Despite their common occurrence, phonolite intrusions in Kaiserstuhl are exposed in walls of the erosional gullies and do not display significant morphological features. Intrusive rocks (essexites, tinguaite, etc.) and deeper diatreme facies are exposed solely in the Schelinger valley; its role is discussed in more detail in the following text. The general character of the landscape suggests that gully erosion only had a limited effect on the morphology, which can thus (even with care) be interpreted in terms of volcanic processes. Overall weak erosion of Kaiserstuhl since the Miocene (ca. 17 Ma) can be explained in terms of its position at the bottom of the Rhine graben, i.e., in an accumulation region close to the erosional base and, therefore, with limited erosion rates, compared to the uplifted (denudation) areas. Although Kaiserstuhl is dominated by lavas, weakly eroded pyroclastic cones of a similar age are also documented elsewhere in the Central European volcanic province (Rappich et al., 2007; Tietz and Büchner, 2015).

Erosional remnants of erupted carbonatites at Kaiserstuhl are found in the western foothills, around the mouth of the broad Schelinger valley, which drains the central part of Kaiserstuhl westward (Fig. 1B). Even though the valley follows the geologically and geophysically documented Schelinger fault (Fig. 1C; Giebel et al., 2019), its open U-shape (Fig. 2A) does not resemble a typical tectonic valley; rather, it suggests significant reshaping by erosion through mass movement (e.g., Chen, 2000; Bouquety et al., 2020, and references therein). In addition, unlike common tectonic valleys, the Schelinger valley does not transect Kaiserstuhl completely, but it extends from its center solely toward the west (Fig. 1B). In the highest part, in the Kaiserstuhl center, the Schelinger valley ends in a 2.5-km-wide amphitheater (Figs. 1C and 2A). There is no evidence of Kaiserstuhl volcano ever having been glaciated. On the other hand, a large accumulation of debrites was documented at the mouth of the Schelinger valley on the western margin of the volcano (Fig. 1C). These debrites were documented at several smaller outcrops in vineyards, road cuts, and small abandoned quarries along the main roads in the Kaiserstuhl foothills. The debrites consist of poorly sorted, matrix-supported polymict volcanogenic conglomerates, forming ~ 2 -m-thick beds at individual outcrops (Fig. 2B). The debrites are unsorted and matrix-supported and contain subrounded to rounded boulders of both eruptive (lavas) and

intrusive rocks of the Kaiserstuhl volcanic complex (Fig. 2C). Locally, finer-grained (sandy) facies remain preserved atop some of the debrite units (Fig. 2C). The presence of volcanoclastic debrites building up the plateau between Niederrotweil and the Outer rift-axis fault was confirmed in borehole 36 (Wimmenauer and Schreiner, 2003, and references therein; Fig. 1C). This drill core documents a > 60 -m-thick sequence dominated by volcanoclastic deposits (Fig. 2D). Despite being described as pyroclastic agglomerates in the original drill log, the detailed description, noting chaotic texture, the absence of sorting, and the presence of rounded blocks of variable dimensions enclosed in a finer matrix, links these deposits with debrites exposed at the surface. Textures of all these debrites (surface exposures and drill core) correspond well with lahar (volcanoclastic debris-flow) deposits (McPhie et al., 1993; Graettinger et al., 2010). Locally, slightly offset, originally jigsaw-fitting angular subclasts were observed in the debrite deposits (Fig. 2E). This specific texture suggests an earlier presence of shattered megablocks with jigsaw-fit textures, which represent a common feature in debris-avalanche deposits (Ui et al., 2000; van Wyk de Vries and Delcamp, 2015). The increasing spacing between individual subclasts of the original megablocks suggests a transition of the debris avalanche into lahars, possibly due to increased water saturation, as the mass flow mixed with available stream water during its passage through the valley (e.g., Bernard et al., 2019). The possible presence of debris-avalanche deposits can be expected also in borehole 36, where, according to the provided description (Wimmenauer and Schreiner, 2003, and references therein), apparently coherent bodies of tephrite (Fig. 2D) comprise frequent joints filled with clayey material. Such textures could correspond to the debris-avalanche matrix that migrated into joints in the shattered megablocks. Therefore, it is likely that at least some of the lahars initiated as debris avalanches derived from a failure of the volcanic edifice (Belousov et al., 1999; Capra et al., 2002; Clavero et al., 2002; van Wyk de Vries and Delcamp, 2015). Such a scenario would explain both the shape of the Schelinger valley, with the wide detachment amphitheater, as well as the lahar distribution.

According to previous reports, the carbonatite pyroclastic deposits in Kaiserstuhl are associated with carbonatite lava exposed on the southern slope of Kirchberg hill (Fig. 1C; Keller, 1981; Wimmenauer and Schreiner, 2003, and references therein). Our examination of this outcrop (sample KS04A) revealed that the rock originally described as carbonatite lava is a well-compacted carbonatite tuff in which interclast voids appear to be significantly reduced (Fig. 3A), most likely

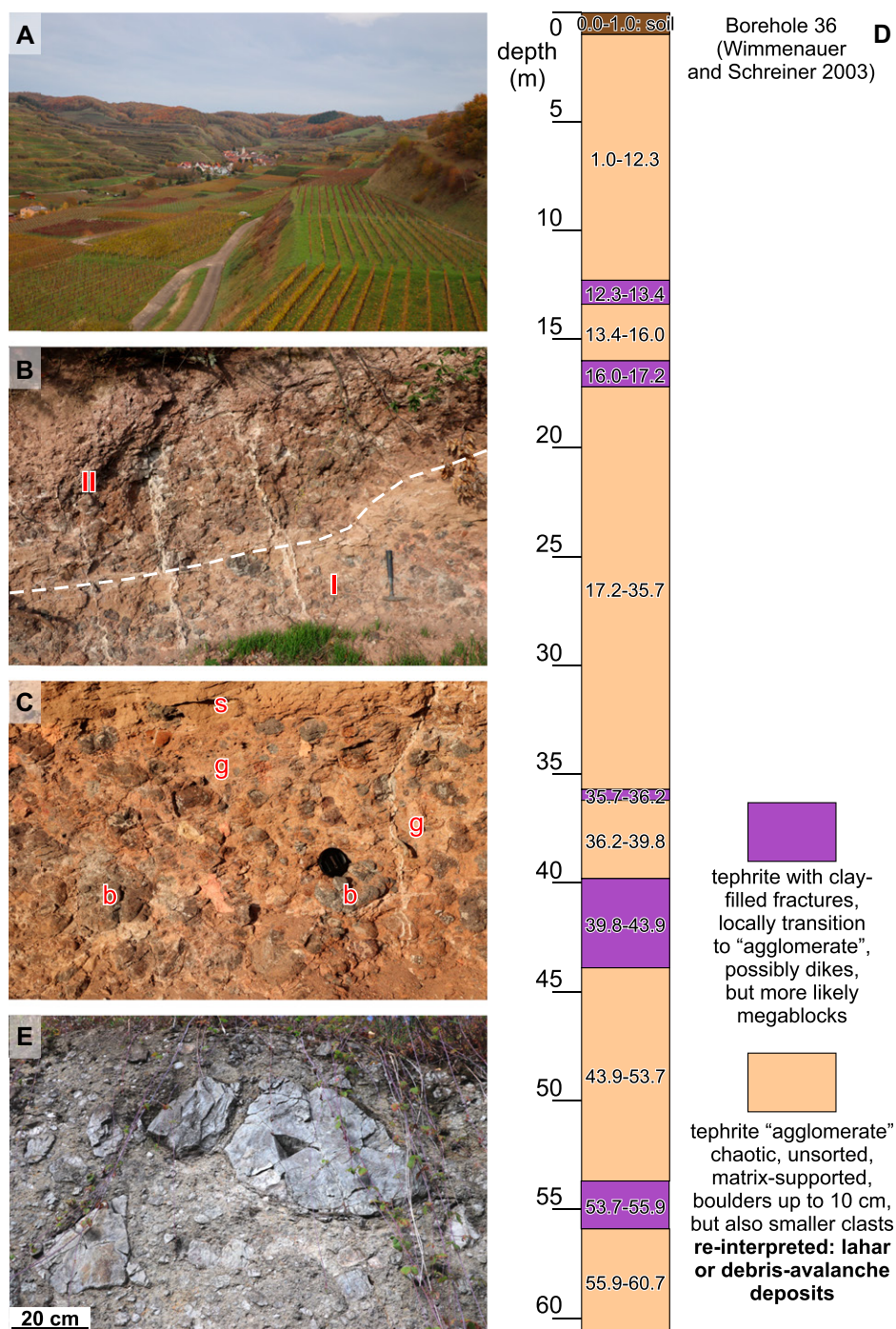


Figure 2. Morphology and studied volcanic facies of Kaiserstuhl volcanic complex (see Fig. 1C for photo locations): (A) Schelinger valley with detachment amphitheater in rear; (B) two units (I and II) of matrix-supported debrites with rounded to subrounded boulders; (C) close-up on unsorted matrix-supported debrite with rounded boulders of lavas (b) enclosed in sandy to clayey groundmass (g) with reworked sandy top (s); (D) reinterpreted profile of drill-hole no. 36 (Wimmenauer and Schreiner, 2003); and (E) larger block indicating the earlier presence of jigsaw-fit texture.

by postdepositional compaction of the lowermost layer of the pyroclastic sequence. Apart from this outcrop, we investigated samples of other out-

crops previously described as carbonatite lava: from the well-known (e.g., Barker, 2007) occurrences of carbonatite pyroclastic deposits on

Henkenberg hill (samples KS05A and KS05B) and an outcrop on Kirchberg hill near the contact with the phonolite intrusion (sample KS12). The carbonatite pyroclastic deposits mainly consist of well-sorted, clast-supported carbonatite tuffs and lapillistones cemented by secondary calcite (Barker, 2007; Fig. 3B). The pyroclast grain size generally varies from ~0.4 mm to ~4 mm (coarse ash to fine lapilli), but individual samples are characterized by very good sorting. Unfortunately, the relations between individual beds or domains with distinct grain size as well as the character of borders (sharp boundary vs. diffuse transition) between different grain-size domains are not observable. All carbonatite pyroclasts, independent of the grain size, are characterized by spherical shape and the absence of vesicles. No fragments of older volcanic rocks or basement country rocks were observed within the carbonatite pyroclastic deposits. The carbonatite tuffs and lapillistones form beds covering the earlier tephrite eruptive facies (Henkenberg), but, more importantly, also lahars in the area of Niederrotweil (Kirchberg). Such a position indicates that the carbonatite explosive eruption occurred following the formation of lahars, and the source vent was not affected by the edifice failure and should thus still be identifiable. In addition, the absence of paleosols or any signs of fossil weathering below the lapillistones precludes a lacuna of any significant duration between deposition of debrites (lahars) and the carbonatite tuffs and lapillistones.

Coherent carbonatites are exposed in the form of numerous bodies in the central part of Kaiserstuhl, in association with the intrusive facies (Fig. 1C). Many of these apparently coherent carbonatites have brecciated textures, where fragmented carbonatites commonly carry angular fragments of other rocks, and are injected and annealed by a younger generation(s) of carbonatites (Fig. 3C; e.g., Baranyi, 1971; Sigmund, 1996; Giebel et al., 2019). The compact appearance of these breccias and the absence of fine-grained clastic groundmass imply multistage intrusive and nonexplosive emplacement of the carbonatite. In contrast, a different type of carbonatite breccia along the detachment escarpment has also been revealed. The carbonatite tuff-breccia occurrences on the slopes of Katharinenberg hill and Orberg hill (Fig. 1C) occur as narrow (few-meter-wide) zones characterized by an open-framework structure (Figs. 3D and 3E), which is partly cemented by secondary calcite. These tuff-breccias consist of angular to subangular fragments of sövite (coarse-grained intrusive/cumulate carbonatite, 2–100 mm in diameter) and spherical pyroclasts (ash to lapilli size, 0.1–4 mm) of porphyritic carbonatite resembling the texture of spherical carbonatite ash and lapilli grains in

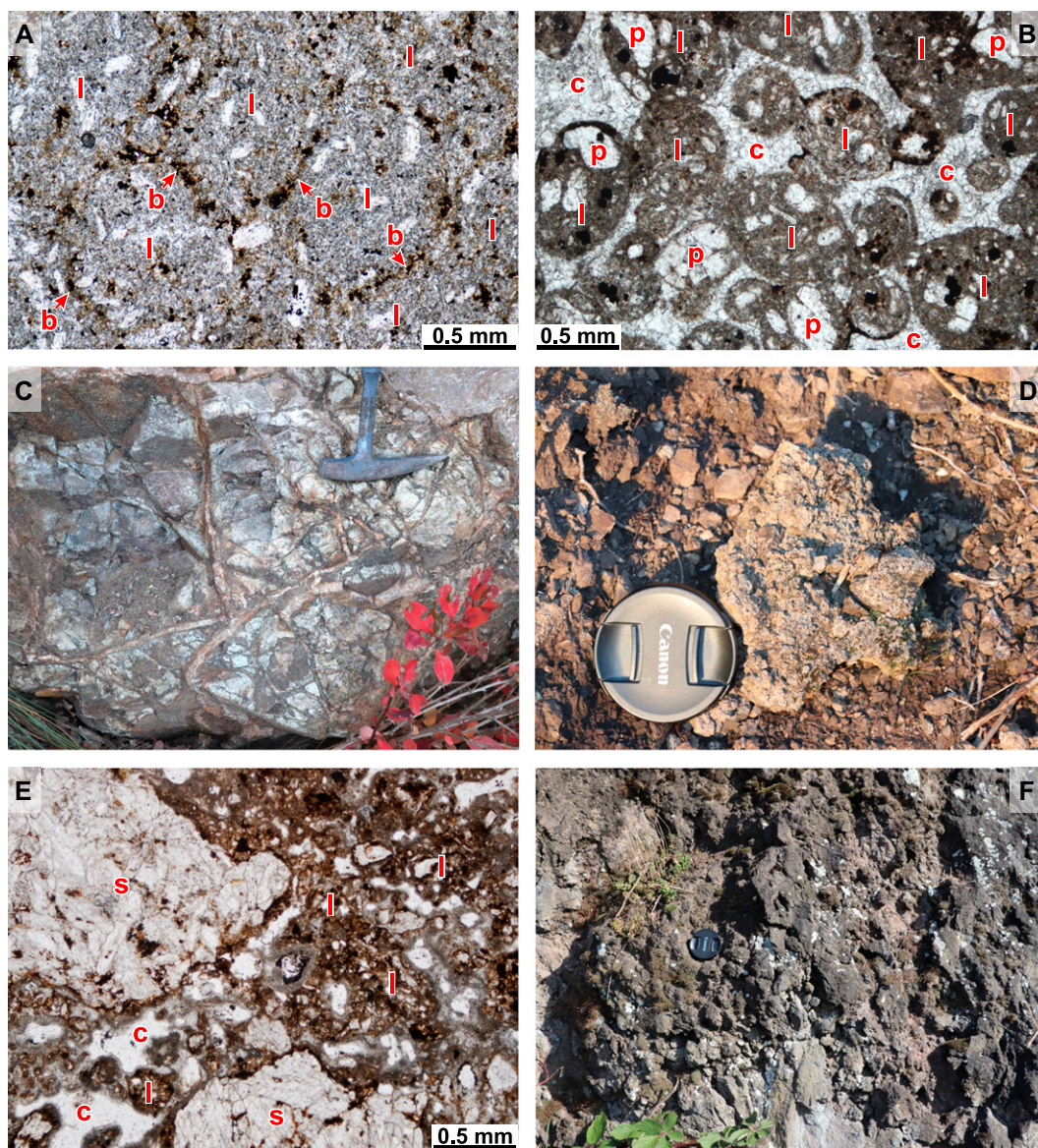


Figure 3. Studied volcanic facies of Kaiserstuhl volcanic complex (see Fig. 1C for photo locations): (A) microphotograph of compacted carbonatite tuff lacking interclast voids (formerly interpreted as lava), with ash grains (l) and their boundaries (b) indicated; (B) microphotograph of the carbonatite tuff showing spherical ash particles (l) of porphyritic (calcite phenocrysts [p]) carbonatite with good sorting and clast-supported texture, indicating pyroclastic fall deposition, and deposit cemented by secondary calcite (c); (C) macrophotograph of intrusive carbonatite breccia carrying angular fragments of silicate rocks and displaying several generations of carbonatite injection; (D) macrophotograph of groundmass in the open-framework texture tuff-breccia; (E) microphotograph of the open-framework tuff-breccia with fragments of sövite (s), and spherical ash grains of porphyritic carbonatite (l) and secondary calcite cement (c); and (F) poorly sorted clast-supported scoria constituting Schlossberg and Schneckenberg scoria cones.

the documented pyroclastic deposits (cf. Fig. 3B). Similar to the carbonatite pyroclastic deposits, the open-framework carbonatite breccias also lack fragments of older volcanic or basement rocks. At Orberg hill, the open-framework tuff-breccia crosscuts the coherent intrusive sövite, but without sharp boundaries; the contacts have the character of a diffuse transition. The margins of the tuff-breccia at Katharinenberg hill are not well exposed. Although lapilli and ash grains in the open-framework tuff-breccia are more irregularly shaped than in the tuff and lapillistones, their similar appearance indicates possible correlation with each other. In addition, the open framework and the absence of the fine-grained fraction (substituted by secondary calcite cement; Fig. 3E) imply explosive fragmentation of the tuff-breccia, with the fine-grained fraction carried away by escaping gases (McPhie et al., 1993).

The eruptive story of the volcanic complex terminated with the growth of two scoria cones (Figs. 1C and 2H), which penetrated and partly buried the lahar deposits.

4.2. Carbonatite Pyroclast Composition

The individual spherical pyroclasts of the carbonatite tuffs and lapillistones have a porphyritic texture (Fig. 3B), which together with the presence of frequent dispersed apatite (Fig. 4A) sets them clearly apart from the pure carbonate (calcite and minor dolomite) secondary sparitic cement. Common phenocrysts (0.05–0.20 mm) in the spherical pyroclasts are represented by calcite, apatite, and magnetite with rims enriched in spinel (MgAl_2O_4 ; Fig. 4B). There are scarce clinopyroxene and melanite phenocrysts, but these phases reach larger diameters (0.5–1 mm).

The secondary sparitic calcite that fills the original voids between individual spherical pyroclasts differs in composition from the magmatic calcite found in the lapilli either in the form of phenocrysts or as a fine-grained groundmass. Whereas the primary magmatic calcite in the spherical pyroclasts is enriched in Sr, the secondary calcite in the cement is very low in Sr but enriched in Mg (see Table 1 for average values; see Supplemental Material Table S1 for full data set¹). This difference is well documented in Mg and Sr distribution

¹Supplemental Material. Table S1. Mineral chemistry data of analyzed carbonates from studied carbonatite pyroclastic deposits. Please visit <https://doi.org/10.1130/GSAB.S.24119295> to access the supplemental material, and contact editing@geosociety.org with any questions.

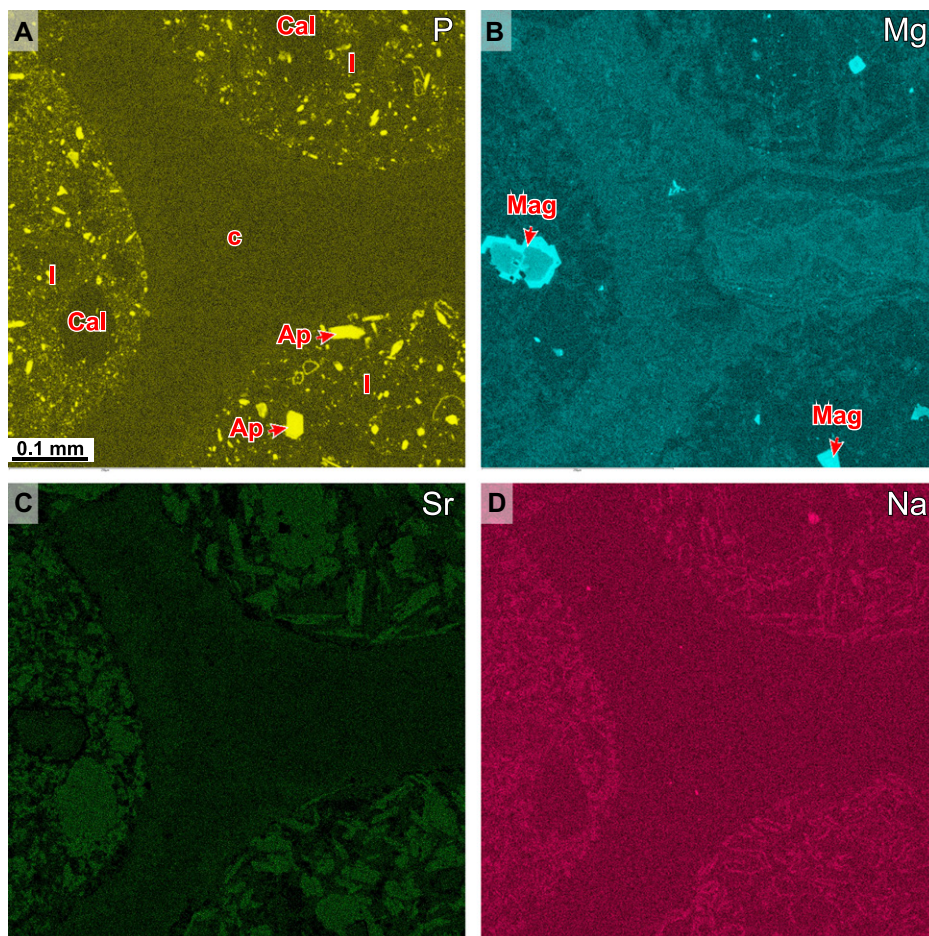


Figure 4. Distribution maps of selected elements in the carbonatite lapillistone from Henkenberg (sample KS05): (A) P; (B) Mg; (C) Sr; and (D) Na. Ap—apatite; Cal—calcite; c—cement; I—lapilli; Mag—magnetite. Scale bar is the same for all figure parts.

maps (Figs. 4B and 4C), and also in the SrO versus MgO binary diagram (Fig. 5A). Within the spherical pyroclasts, both the calcite phenocrysts as well as small crystals in the groundmass are characterized by Na-enrichment in the outermost rims. This enrichment is well documented in the Na-distribution map (Fig. 4D), although we note that the rim was too thin for a detailed spot analysis. Nonetheless, the highest

Na₂O content in the calcite crystal rim obtained from microprobe analysis exceeded 0.8 wt% (Table S1).

The ⁸⁷Sr/⁸⁶Sr determinations on bulk rock, separated lapilli, and secondary cement from sample KS12 from Kirchberg were indistinguishable within analytical uncertainty, i.e., 0.70362–0.70363 (Table 1). These values fit in the range of ⁸⁷Sr/⁸⁶Sr values between 0.7036 and

0.7040 reported for Kaiserstuhl intrusive carbonatites by Schleicher et al. (1990).

In contrast to Sr isotope ratios, the stable C and O isotope compositions differ between the pyroclastic rocks and intrusive carbonatites. The Kaiserstuhl intrusive carbonatites (samples KS01, KS03B, KS03D, and KS03E in Table 2) fit well in the field of primary igneous carbonatites (sensu Taylor et al., 1967), whereas the pyroclastic carbonatites deviated toward lighter carbon ($\delta^{13}\text{C}$ from -9.2‰ to -8.0‰) and, at the same time, ^{18}O -enriched compositions ($\delta^{18}\text{O}$ from 15.9‰ to 16.5‰ ; Table 2; Fig. 5B). Small differences in $\delta^{13}\text{C}$ were observed between pyroclastic samples deposited on the lahar fan (both localities on Kirchberg, $\sim -8.0\text{‰}$) and the samples collected from the cover of the prelahar edifice (Henkenberg, $\sim -9.0\text{‰}$). The secondary cement in the lapillistone (coarser-grained facies were processed because distinct domains could be separated more easily) covering the lahar fan (Kirchberg) did not differ compositionally from the lapilli, whereas a significant shift in both carbon ($\delta^{13}\text{C}$ from -11.8‰ to -11.3‰) and oxygen ($\delta^{18}\text{O}$ from 24.0‰ to 24.2‰) was observed in the case of Henkenberg lapillistone cement. The values and also the shift between lapilli and cement in the samples from Henkenberg correspond well with the earlier results obtained from this locality (Hubberten et al., 1988; Barker, 2007). In addition, clumped isotope Δ_{638} values (Table 2) of secondary cements were higher than values of separated pyroclasts ($0.576\text{‰} \pm 0.004\text{‰}$ vs. $0.302\text{‰} \pm 0.020\text{‰}$ and $0.448\text{‰} \pm 0.015\text{‰}$). The higher Δ_{638} value of the cement sample corresponds to a lower temperature of $\sim 31^\circ\text{C}$ compared to the much higher temperatures of the measured separated pyroclasts of 241°C and 91°C , respectively.

5. DISCUSSION

5.1. Eruption Style and Carbonatite Fragmentation

The character and geometry of pyroclasts are widely used tools in deciphering the eruption style and process leading to magma fragmentation (e.g., Fisher and Schmincke, 1984; Cas and Wright, 1988; McPhie et al., 1993). First, we focus on the tuff-breccias. Their monomict composition, consisting solely of calciocarbonatite clasts and lacking any fragments of older volcanic or basement rocks, strongly contrasts with diatreme breccias of common phreatomagmatic maar-diatreme volcanoes or kimberlite pipes (e.g., Lorenz and Kurszlaukis, 2007; Kjarsgaard et al., 2022; Walter et al., 2023). The monomict composition together with the diffuse transition between open-framework tuff-breccia and

TABLE 1. COMPOSITION OF CARBONATE PHASES FROM STUDIED PYROCLASTIC DEPOSITS OF KAISERSTUHL VOLCANIC COMPLEX*

Rock sample:	KS05A				
	Calcite	Calcite	Calcite	Calcite	Dolomite
Mineral:	L-x	L-p	L-g	C	C
Type:	L-x	L-p	L-g	C	C
n:	4	9	9	10	1
FeO	0.04		0.01	0.34	17.52
MgO	0.85	0.04			
CaO	53.38	52.23	53.32	53.46	32.43
SrO		1.21	1.18	0.01	0.53
Total	54.27	53.71	54.52	53.81	50.47

Note: L-p—phenocryst in pyroclast; L-g—pyroclast groundmass; L-x—glomerocryst with noncarbonate mineral phase; C—cement in between pyroclasts; n—number of analyses.

*Values are in wt%.

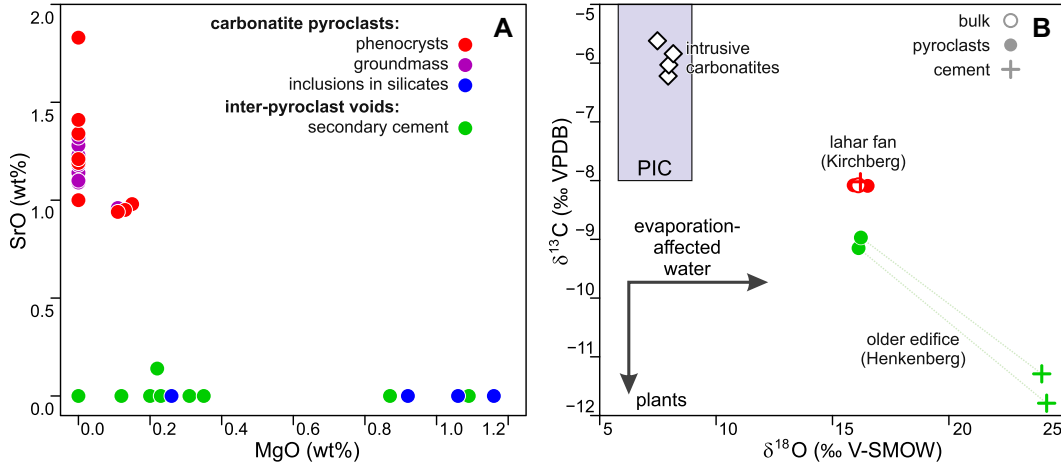


Figure 5. Composition of studied carbonatite pyroclastic rocks from Kaiserstuhl volcanic complex: (A) SrO vs. MgO binary diagram and (B) stable C and O isotope compositions. PIC—primary igneous carbonatites; VPDB—Vienna Pee Dee belemnite; VSMOW—Vienna standard mean ocean water.

intrusive carbonatite at the Orberg hill provide strong evidence that the breccia was derived and erupted from the intrusive carbonatite. There is no lithological evidence of significant influence of external water on the eruption dynamics.

Pyroclastic deposits consisting of poorly vesiculated juvenile fragments of silicate magmatic rock and lacking significant amounts of basement-rock xenoliths provide evidence of hydromagmatic fragmentation in a Surtseyan-style eruption (e.g., Kokelaar, 1983; Cole et al., 2001; Murtagh and White, 2013; Németh and Kósik, 2020). On the other hand, fragments of the hydromagmatic hyalo-tuffs are (besides low vesicularity and a hypocrySTALLINE texture) commonly characterized by irregular shapes, combining concave (vesicle walls) and straight (brittle fragmentation during quenching) grain boundaries. Spherical shapes of ash grains or lapilli usually require reshaping of the melt shreds by surface tension, which requires very low viscosity, allowing for faster changes of the shape than cooling and freezing of the clast. At certain conditions, spherical lapilli can also be formed from silicate melts of extremely low viscosity (e.g., Jones et al., 2022, and references therein). Experiments of Comida et al. (2023)

with low-viscosity silicate melts confirmed the formation of spherical particles during Hawaiian-style eruptions as a result of melt sprayed by pressurized (rapidly escaping) gas. Spherical particles of silicate melts were also obtained during experimental phreatomagmatic eruptions (Zimanowski et al., 1997), though in a mixture with other geometries combined with more intense fragmentation, whereas the investigated carbonatite pyroclastic deposits consist solely of spherical pyroclasts.

Calcio-carbonatite viscosity at 800 °C (near solidus according to Podborodnikov et al., 2018) and near-atmospheric pressure was calculated to be 0.08 Pa·s (Wolff, 1994; Jones et al., 2013). Although the viscosity of natro-carbonatite is even lower (0.008 Pa·s) and very close to the viscosity of water (0.001 Pa·s at standard temperature and pressure [STP]), all carbonatites were characterized by viscosity far below values of even very basic and high-temperature silicate melts (Kono et al., 2014). Viscosity of basanitic lavas of Cumbre Vieja (La Palma, Canary Islands), erupted in 2021, varied in the range of 10–160 Pa·s depending on temperature (1150–1200 °C) and slight changes in composition (Castro and Feisel, 2022). These values were

predicted earlier on the basis of experiments and models by Giordano et al. (2008). Thus, calcio-carbonatite viscosity is 100–2000 times lower than the viscosity of basanite under comparable conditions, which significantly influences the behavior of carbonatite pyroclasts during eruption. The extremely low viscosity of carbonatites, which is not significantly dependent on temperature until the freezing point, also enables effective reshaping of the melt shreds forced by surface tension. When supported by very low viscosity, this process is faster than freezing of the melt shreds and may result in spherical pyroclasts devoid of vesicles, as observed in all documented carbonatite pyroclastic deposits worldwide (e.g., Keller, 1981; Rosatelli et al., 2003; Barker, 2007; Reguir et al., 2008; Mourão et al., 2010; Campeny et al., 2014).

Only a handful of experiments have been conducted with carbonatite melts, represented solely by alkali carbonatites. Experiments by Zimanowski et al. (1986) focused on phreatomagmatic (magma-water or fuel-coolant interaction) explosions producing spherical pyroclasts, but according to their observations, the CO_2 exsolution appears to have suppressed any magma-water interaction effect under test conditions.

TABLE 2. ISOTOPIC COMPOSITIONS OF STUDIED COHERENT AND PYROCLASTIC CARBONATITE ROCKS FROM KAISERSTUHL VOLCANIC COMPLEX

Sample	Locality	Latitude (°N)	Longitude (°E)	Type	$\delta^{13}\text{C}$ (‰, VPDB)	$\delta^{18}\text{O}$ (‰, VSMOW)	Δ_{638} (‰, CDES 90)	Δ_{638} 1 SE (‰)	Δ_{638} T (°C)	$^{87}\text{Sr}/^{86}\text{Sr}$	1 SD	N	2 SE
KS01	Badloch	48.09282	7.67297	Intrusive	-6.2	7.9							
KS03B	Ohrberg	48.10376	7.69075	Intrusive	-6.0	8.0							
KS03D	Ohrberg	48.10409	7.68983	Intrusive	-5.6	7.5							
KS03E	Ohrberg	48.10488	7.69204	Intrusive	-5.8	8.2							
KS04A	Kirchberg	48.08151	7.61382	Pyroclast	-8.1	15.9							
KS12-L	Kirchberg	48.08216	7.61493	Pyroclast	-8.1	16.5	0.448	0.015	92	0.703621	0.000046	97 of 100	0.000009
KS12-C	Kirchberg	48.08216	7.61493	Cement	-8.0	16.2				0.703622	0.000050	99 of 100	0.000010
KS12-B	Kirchberg	48.08216	7.61493	Bulk rock	-8.1	16.1				0.703627	0.000049	97 of 100	0.000010
KS05A-C	Henkenberg	48.09407	7.60874	Cement	-11.8	24.2	0.576	0.004	31				
KS05A-L	Henkenberg	48.09407	7.60874	Pyroclast	-9.2	16.1	0.302	0.020	241				
KS05b-C	Henkenberg	48.09407	7.60874	Cement	-11.3	24.0							
KS05B-L	Henkenberg	48.09407	7.60874	Pyroclast	-9.0	16.2							

Note: Coordinate system is WGS84, decimal degrees. VPDB—Vienna Pee Dee belemnite; VSMOW—Vienna standard mean ocean water; CDES—carbon dioxide equilibrium scale at a reaction temperature of 90 °C; SE—standard error; SD—standard deviation.

Melts with very low viscosity may, in all likelihood, still produce spherical particles during the interaction with water under conditions of noneffective cooling (small amounts of water or just above the explosion site; Zimanowski et al., 1986). Nonetheless, the absence of wall-rock xenoliths in both the vent breccia and the carbonatite pyroclastic deposits makes a phreatomagmatic scenario for the Kaiserstuhl pyroclastic deposits less likely. On the other hand, reaction with small amounts of surface water represented by a crater lake (hydromagmatic eruptions) cannot be excluded. The amount of escaping gas spraying the low-viscosity carbonatite melt appears to be the crucial factor in formation of spherical carbonatite pyroclasts.

5.2. Conditions of Carbonatite Pyroclast Formation and Deposition

The origin of the carbonatite pyroclastic deposits and conditions of their deposition and cementation can be further constrained by stable C and O and radiogenic Sr isotopic compositions. The main assumption qualifying the carbonatite lapilli for further genetic interpretation is the absence of postdepositional recrystallization or reequilibration of isotope systems with the new environment. The original porphyritic texture of the carbonatite pyroclasts contrasts with the sparitic texture of the cement (Fig. 3B), and the carefully separated pyroclasts devoid of any traces of cement did not display any signs of recrystallization. In addition, the presence of Na-enriched rims enveloping all fractions of calcite crystals in the lapilli (Fig. 4D) excludes any possible ion exchange (such as calcification of different carbonate phase; e.g., Deans and Roberts, 1984), as the crystal rims would be the first phase affected by such a process. The data obtained from the carbonatite pyroclasts can thus be considered reliable. Further evidence for the origin of the lapilli comes from the clumped isotope data. The determined clumped isotope temperature of 241 °C for KS05A-L suggests rapid cooling, preventing solid-state isotope reordering. These data also exemplify the need for careful separation of primary carbonatite pyroclasts from secondary cement when studying carbonatite pyroclastic deposits.

The very narrow $\delta^{18}\text{O}$ variation (15.9‰–16.5‰) in carbonatite pyroclasts from this study suggests a distinctive shift from the original mantle values of the intrusive Kaiserstuhl carbonatites, here represented by samples KS01, KS03B, KS03D, and KS03E with $\delta^{18}\text{O}$ values ranging between 7.5‰ and 8.2‰. This $\delta^{18}\text{O}$ shift of ~8‰ is not likely to be related to the transport, deposition, or cementation of the pyroclasts because these processes would lead to

different extents of oxygen isotope shift. Instead, we posit that this uniform ^{18}O enrichment must have taken place prior to the eruption. The ^{18}O -enriched character of the carbonatite pyroclasts does not fit well with the potential role of infiltration of meteoric water that is isotopically much lighter than the intrusive carbonatites themselves. Instead, it points toward residual water that was affected by progressive evaporation. Evaporative oxygen isotope fractionation toward an ^{18}O -depleted signature in vapor versus ^{18}O -enriched compositions in residual brines of several per mil units compared to source-crater meteoric lake waters was shown earlier (Rowe, 1994; Varekamp and Kreulen, 2000). We anticipate that the oxygen isotope relation among individual components of the carbonatite pyroclastic deposits could be explained in terms of open-system hydrothermal circulation with the escape of isotopically light vapor from the volcano's crater and subsequent reaction of the residual ^{18}O -enriched water with the topmost parts of the fresh carbonatite intrusion. This process would shift the oxygen isotopic composition toward higher $\delta^{18}\text{O}$, with homogeneous values among subsequently sprayed and dispersed pyroclasts.

The difference in $\delta^{13}\text{C}$ between Henkenberg and Kirchberg requires another explanation. Although $\delta^{13}\text{C}$ values in both localities are shifted toward ^{13}C -depleted compositions compared to the intrusive carbonatite $^{13}\text{C}/^{12}\text{C}$ signature ($\delta^{13}\text{C}$ from -6.2‰ to -5.6‰; Table 2), this shift is more pronounced in the case of Henkenberg ($\delta^{13}\text{C}$ of ~-9‰) compared to Kirchberg ($\delta^{13}\text{C}$ of ~-8‰; Fig. 5B; Table 2). The shift toward isotopically lighter carbon cannot be explained in terms of atmospheric CO_2 involvement but rather points to the involvement of biogenic carbon. The difference between both localities suggests a significant role of postdepositional carbon reequilibration under distinct morphological conditions at each locality. Both occurrences of carbonatite pyroclastic deposits differ in their substrata (i.e., in the rocks covered by pyroclastic deposits) and also in the time provided for pre-eruptive vegetation to grow. Whereas the carbonatite tephra in the area of Kirchberg was deposited directly on fresh debrites (lahar and debris-avalanche deposits), the identical pyroclastic deposit in the Henkenberg area fell on long-exposed and probably vegetated remnants of the earlier tephrite shield volcano (Fig. 1C). Although the debris avalanches and lahars incorporated a significant mass of vegetation during their slide down the volcano slope (its decomposition provided some amount of light carbon), their surface at the time of carbonatite lapilli deposition was lacking any vegetation cover. In contrast, more distal parts at Henkenberg were represented by the surface of the Kaiserstuhl

lavas, at that time vegetated and providing a significant proportion of ^{13}C -depleted carbon to reequilibrate the carbon isotope composition of the pyroclastic deposit.

An additional shift in stable isotope compositions is also apparent between the cement and lapilli at Henkenberg, while the cement at Kirchberg does not differ compositionally from lapilli (Fig. 5B). The more pronounced shift toward heavier oxygen and lighter carbon composition in the Henkenberg cement indicates the additional contribution of evaporation-modified water and rich vegetation, probably suggesting deposition and cementation of the Henkenberg pyroclastic deposits in vegetation-rich shallow (evaporating) ponds or marshes.

5.3. Trigger of the Volcano Instability

The superposition of carbonatite lapillistones directly on the surface of lahar deposits and the alignment of the open-framework tuff-breccia occurrences along the detachment scarp collectively provide unequivocal field evidence for the close temporal relation between carbonatite eruption with its products (open-framework tuff-breccias and tuffs to lapillistones) and volcano flank failure and its deposits (debris-avalanche deposits and lahars; Fig. 1C).

A volcano flank failure triggering an explosive eruption is a well-documented scenario for the prehistorical eruption of the Soufrière volcano, Guadeloupe (Boudon et al., 1984), and was even eye-witnessed for the events of Bezymianny in 1956 (Belousov, 1996) and Mount St. Helens in 1980 (e.g., Reid et al., 2010; Walter, 2011). These events represent examples of differentiated calc-alkaline volcanoes in convergent settings. Magma in such volcanic systems is rich in volatiles (in particular, water), resulting in (1) high hydrothermal alteration potential and (2) high explosive potential (large volume of expandable gases). Flank failure, usually enabled by intense hydrothermal alteration of the volcano interior (e.g., van Wyk de Vries et al., 2000) or even overpressurization of the hydrothermal system (Reid, 2004), may release the pressure under which a geochemically evolved cryptodome sits inside the volcano edifice, resulting in decompression exsolution of the magmatic gases and explosive eruption.

Despite distinct mineralogy and geochemistry, silicate alkaline-carbonatite volcanoes may share some important physical properties with arc-related silicic volcanoes, resulting in partly comparable eruptive scenarios: (1) Carbonatite magmas are accompanied by complex fluid systems (e.g., Rankin, 2005; Walter et al., 2020, 2021), which commonly lead to pervasive alteration and metasomatic overprinting of the origi-

nal rock environment (Kresten and Morogan, 1986; Elliott et al., 2018; Liu et al., 2018), and (2) although intraplate or continental rift–related alkaline magmas are generally low in volatiles, carbonatites themselves represent a crucial reservoir of volatiles (namely CO_2 , F). Because carbonatites are dominated by igneous carbonates, the amount of potentially available CO_2 is enormous (at full decomposition, 1000 kg of CaCO_3 releases 245 m^3 of CO_2 at STP, and this volume increases significantly with temperature).

Flank failures have been documented for carbonatite volcanoes in the East African Rift, e.g., Oldoinyo Lengai and Kerimasi (Kervyn et al., 2008; Reguir et al., 2008; Delcamp et al., 2016), but the association of sector collapse with subsequent carbonatite explosive eruption was not documented. In addition, both the Oldoinyo Lengai and Kerimasi volcanoes have been issuing natrocarbonatites, i.e., erupted fractionated members of primordial carbonatite magma (Weidendorfer et al., 2017), the surface physical properties of which are distinctively different from typical calciocarbonatite. The calciocarbonatites that intruded repeatedly into the central part of Kaiserstuhl (Wimmenauer and Schreiner, 2003; Walter et al., 2018; Giebel et al., 2019) were associated with extensive fluid activity causing pervasive alteration of the volcano interior (e.g., Walter et al., 2018). The most common alteration associated with carbonatites is fenitization, i.e., alteration associated with vast enrichment in alkalis, namely potassium (e.g., Kresten and Morogan, 1986; Elliott et al., 2018; Liu et al., 2018). As a result of the massive supply of K, the fenitized rock is characterized by the replacement of the original mineral assemblage by K-feldspar (in Si-rich rocks: e.g.,

Kresten and Morogan, 1986; Morogan, 1989) or phlogopite (in Mg-rich rocks: e.g., Holub et al., 2010; Viladkar, 2015; Ackerman et al., 2017). Unfortunately, disentangling the alkali enrichments in the originally alkali-rich rocks may be difficult due to the presence of primary alkali-rich phases. Despite some doubts about the role of alteration in the central part of Kaiserstuhl, hydrothermal alteration of the originally solid rocks has been documented at several places (e.g., Weisenberger et al., 2014). Moreover, a systematic geophysical survey has revealed strong fenitization in the central part of Kaiserstuhl based on K/Th maps (Brauch et al., 2018). The K/Th ratio, in contrast to simple K contents, separates the effects of fenitization (enriched in K but not in Th) from the presence of phonolitic bodies (enriched in both K and Th). In addition, we have also investigated a potentially fenitized phonolite from Orberg (north of quarry V) using a microprobe. Although no significant compositional shifts were identified in the petrography or bulk-rock chemistry, the microprobe observations revealed massive replacement of primary sanidine with a secondary mixture of microcline and sericite (Fig. 6), suggesting a significant supply of K-rich fluids. Indirect evidence of hydrothermal activity is also provided by heavier stable O isotope signatures of the carbonatite lapilli (see section 5.2 of the Discussion).

The alteration together with the vertical offset along the rift-related Tuniberg fault created conditions that predisposed the edifice to subsequent flank failure. The total vertical displacement on the Tuniberg fault reaches 1000 m to the north and 3000 m to the south of Kaiserstuhl, respectively (Giebel et al., 2019, and references therein); at least several hundred meters

of movement occurred during the development of Kaiserstuhl (Figs. 1C and 7B). Tectonic activity associated with Rhine graben subsidence explains the formation of the topography required for edifice instability, because the shield volcanoes, including Kaiserstuhl, are characterized by gently dipping slopes built from effusions of low-viscosity lavas. An edifice failure occurring on a carbonatite-hosting alkaline volcano may uncover a carbonatite intrusion, abruptly changing its physical conditions and allowing it to erupt (Figs. 7C and 7D). This proposed scenario of volcano failure leading to carbonatite eruption (Fig. 7) was also visualized in a near-realistic three-dimensional animation following the concepts developed by Rappich et al. (2017) and is publicly available at <https://www.youtube.com/watch?v=GSNiFXzsCHA>.

5.4. Implications for the Eruption of a Calciocarbonatite

Although some recent authors (e.g., Weidendorfer et al., 2017; Yaxley et al., 2022) considered calciocarbonatites to be solely cumulate rocks, the observed porphyritic textures (Fig. 3B) indicate that the calciocarbonatite pyroclasts at Kaiserstuhl formed from a melt at conditions between solidus and liquidus. Although the carbonatite melt contained some Na_2O , incorporated into late-stage crystallized calcite (Fig. 4D), the entire system was dominantly calcic. Experiments carried out for various pressure conditions have indicated a systematic decrease in solidus temperature for CaCO_3 with decreasing pressure (e.g., Cooper et al., 1975; Ivanov and Deutsch, 2002; Shatskiy et al., 2013). Podborodnikov et al. (2018) experimentally determined a solidus temperature of 813 °C at 0.1 GPa. This means that decompressed calciocarbonatite melt following flank failure would have occurred at a set of pressure-temperature conditions where the CaCO_3 phase is unstable, resulting in its rapid breakdown, according to the experiments of Karunadasa et al. (2019). The porphyritic textures of the carbonatite pyroclasts (calcite phenocrysts in calcite groundmass) from Kaiserstuhl indicate that the pyroclasts were rapidly chilled from a temperature somewhere between the liquidus and solidus, which corresponds to the conditions for the high-rate CaCO_3 breakdown reaction (>790 °C; Karunadasa et al., 2019). As a consequence, eruption of calciocarbonatite lava is highly unlikely because its cooling rate is too sluggish compared to the high rate of the CaCO_3 breakdown reaction. In contrast, gas expansion during an explosive eruption, combined with a large cooling surface area, would

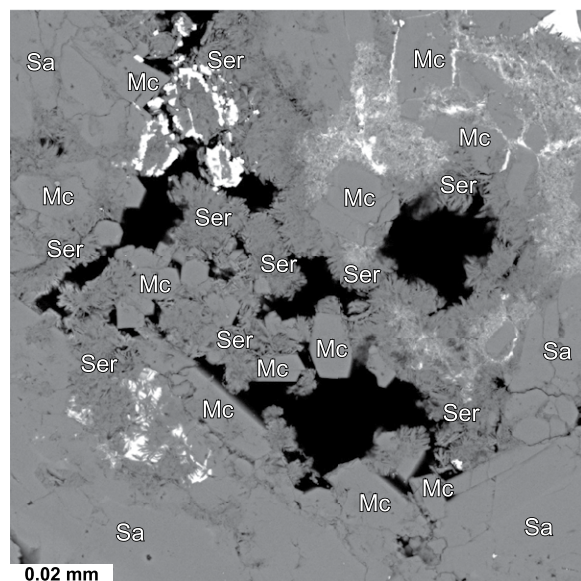


Figure 6. Backscattered-electron image of the fenitized phonolite from Orberg. Mc—microcline; Sa—sanidine; Ser—sericite.

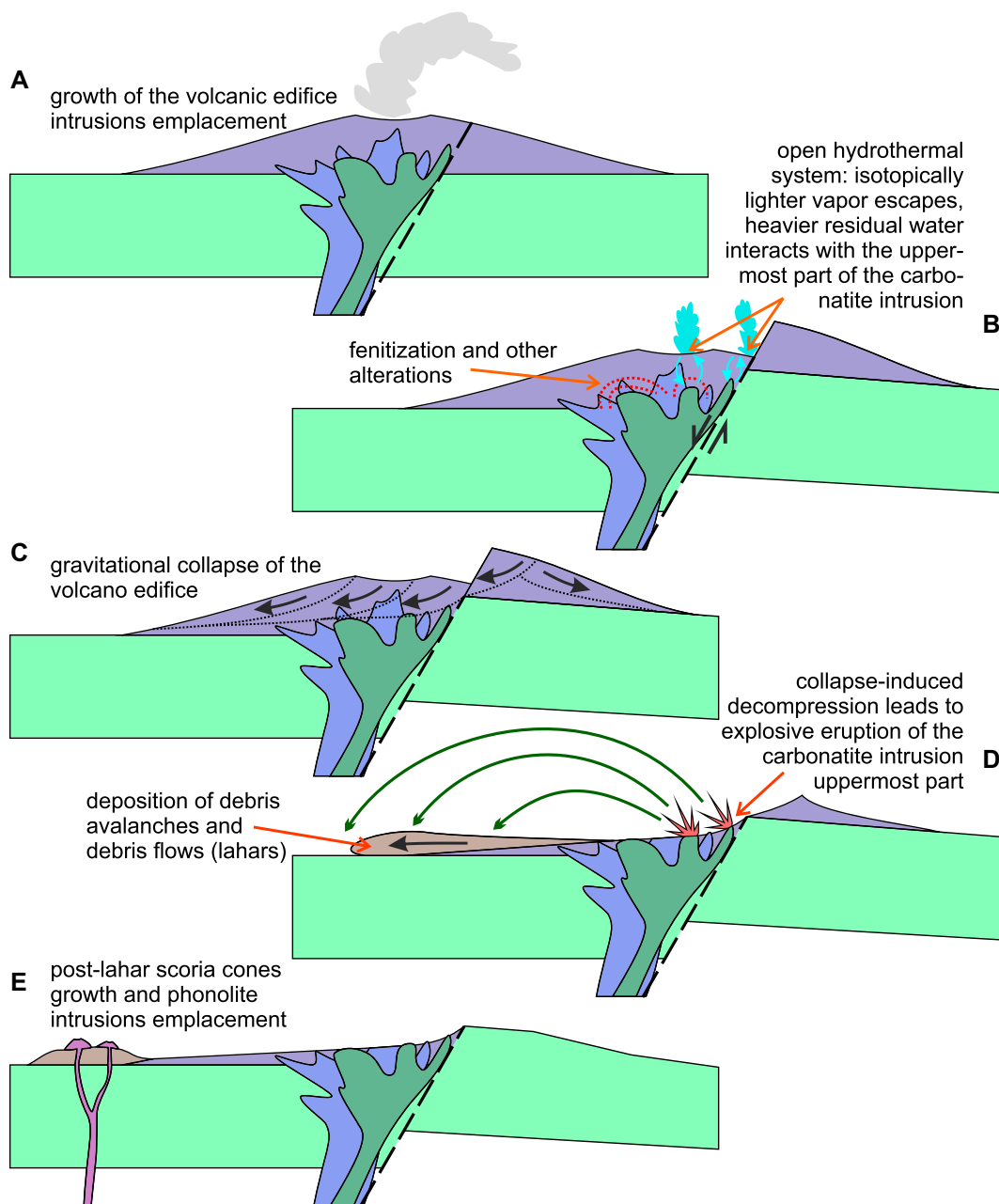


Figure 7. Interpreted eruption history of the Kaiserstuhl volcanic complex: (A) growth of a shield volcano with central intrusion complex; (B) destabilization of the volcanic core due to rift-related tectonics (rift-related Tuniberg fault) and carbonatite-related alterations; (C) flank failure of the volcano; (D) exposure of the partially solidified carbonatite intrusions leads to decompression-triggered explosive eruption of the calciocarbonatite, depositing its pyroclastic fall deposits onto a lahar fan; and (E) late-stage scoria cones penetrating and covering the lahar fan.

lead to rapid chilling of erupted pyroclasts (but after their shaping to spherical form driven by the surface tension).

If the carbonatite system is not easily capable of segregating natrocarbonatite magma, which is more prone to surface eruptions (Oldoinyo Lengai), an edifice failure instantly exposing partly cooled calciocarbonatite intrusions (but still above the solidus temperature) may represent an alternative important process triggering calciocarbonatite eruptions. The Kaiserstuhl example may then explain why the surface-erupted calciocarbonatites are globally so subordinate. The absence of edifice failure, which would have to occur in the time interval during which the

calciocarbonatite intrusion was in the required temperature range, may also explain the fact that many alkaline volcanoes that are expected to, or have already, exposed calciocarbonatite intrusions are not associated with surface-erupted calciocarbonatites (e.g., Napak, Toro Ankole, Virunga, all Uganda—Simonetti and Bell, 1994; Pitcavage et al., 2021; Doupovské hory Mountains in the Ohře Rift, Czech Republic—Holub et al., 2010).

6. CONCLUSIONS

The volcanic evolution of the Kaiserstuhl volcano remained, to a great extent, an overlooked

problem of this interesting magmatic system despite extensive studies on its mineralogy, magmatic petrology, and geochemistry. Our research demonstrates the importance of a basic textural-based approach when studying the evolution of magmatic systems comprising multiple volcanic facies. The principal conclusions of our investigations can be summarized as follows:

(1) The Miocene Kaiserstuhl volcano likely experienced calciocarbonatite eruption following edifice failure of the volcano that exposed the intrusive system.

(2) The monomict composition of the carbonatite pyroclastic deposits is inconsistent with a phreatomagmatic style of eruption, although lim-

ited influence of surface water (hydromagmatic scenario) on the eruption cannot be excluded.

(3) Spherical and vesicle-free carbonatite pyroclasts most likely resulted from reshaping of extremely low-viscosity melt shreds forced by surface tension, or direct spraying of the melt by rapidly escaping gases.

(4) Calciocarbonatite eruption requires rapid unloading of the overburden of an intrusion, such that cooling outpaces the rapid carbonate breakdown kinetics.

(5) The absence of edifice failure features on alkaline volcanoes may then explain the global scarcity of erupted calciocarbonatites.

(6) The physical volcanology of carbonatite complexes has not yet attracted intensive attention despite the fact that understanding of the eruptive evolution may significantly contribute to improved understanding of the entire magmatic system.

ACKNOWLEDGMENTS

This work was funded by the Czech Science Foundation project 19-29124X. Light detection and ranging (LiDAR)-based topography data were provided by the Landesamt für Geoinformation und Landentwicklung of Baden-Württemberg (Baden-Württemberg State Office of Geoinformation and Land Development). Martin Lisec is acknowledged for creation of the three-dimensional animation. The manuscript benefited from constructive comments by Benjamin van Wyk de Vries, Volker Lorenz, Science Editor Mihai Ducea, and Associate Editor Michael Ort. We also acknowledge comments by an anonymous reviewer of an earlier version of the manuscript.

REFERENCES CITED

- Ackerman, L., Magna, T., Rappich, V., Upadhyay, D., Krátký, O., Čejková, B., Erban, V., Kochergina, Y.V., and Hrstka, T., 2017, Contrasting petrogenesis of spatially related carbonatites from Samalpatti and Sevattur, Tamil Nadu, India: Lithos, v. 284–285, p. 257–275, <https://doi.org/10.1016/j.lithos.2017.03.029>.
- Anderson, N.T., Kelson, J.R., Kele, S., Daëron, M., Bonifacie, M., Horita, J., Mackey, T.J., John, C.M., Kluge, T., Petschnig, P., Jost, A.B., Huntington, K.W., Bernasconi, S.M., and Bergmann, K.D., 2021, A unified clumped isotope thermometer calibration (0.5–1100°C) using carbonate-based standardization: Geophysical Research Letters, v. 48, <https://doi.org/10.1029/2020GL092069>.
- Baranyi, I., 1971, Petrographie und Geochemie der subvulkanischen Breccien des Kaiserstuhls und seiner Umgebung [Ph.D. dissertation]: Freiburg, Germany, University of Freiburg, 156 p.
- Barker, D.S., 2007, Origin of cementing calcite in “carbonatite” tuffs: Geology, v. 35, p. 371–374, <https://doi.org/10.1130/G22957A.1>.
- Beccaleto, L., Capar, L., Cruz-Mermey, D., Rupf, I., Nitsch, E., Oliviero, G., Elsass, P., Perrin, A., and Stephane, M., 2010, The GEORG project—Geological Potential of the Upper Rhine Graben: Situation, goals and first scientific results, in 23ème Réunion des Sciences de la Terre (RST2010): Bordeaux, France, Bureau de Recherches Géologiques et Minières (BRGM), abstract hal-00642768.
- Belousov, A., 1996, Deposits of the 30 March 1956 directed blast at Bezymianny volcano, Kamchatka, Russia: Bulletin of Volcanology, v. 57, p. 649–662, <https://doi.org/10.1007/s004450050118>.
- Belousov, A., Belousova, M., and Voight, B., 1999, Multiple edifice failures, debris avalanches and associated eruptions in the Holocene history of Shiveluch volcano, Kamchatka, Russia: Bulletin of Volcanology, v. 61, p. 324–342, <https://doi.org/10.1007/s004450050300>.
- Bernard, K., van Wyk de Vries, B., and Thouret, J.C., 2019, Fault textures in volcanic debris-avalanche deposits and transformations into lahars: The Pichu Pichu thrust lobes in south Peru compared to worldwide avalanche deposits: Journal of Volcanology and Geothermal Research, v. 371, p. 116–136, <https://doi.org/10.1016/j.jvolgeores.2019.01.008>.
- Bernasconi, S.M., et al., 2021, InterCarb: A community effort to improve inter-laboratory standardization of the carbonate clumped isotope thermometer using carbonate standards: Geochemistry, Geophysics, Geosystems, v. 22, <https://doi.org/10.1029/2020GC009588>.
- Bizzarro, M., Simonetti, A., Stevenson, R.K., and David, J., 2002, Hf isotope evidence for a hidden mantle reservoir: Geology, v. 30, p. 771–774, [https://doi.org/10.1130/0091-7613\(2002\)030<0771:HIEFAH>2.0.CO;2](https://doi.org/10.1130/0091-7613(2002)030<0771:HIEFAH>2.0.CO;2).
- Boudon, G., Semet, M.P., and Vincent, P.M., 1984, Flank failure-directed blast eruption at Soufrière, Guadeloupe, French West Indies: A 3,000-yr-old Mt. St. Helens?: Geology, v. 12, p. 350–353, [https://doi.org/10.1130/0091-7613\(1984\)12<350:FFBEAS>2.0.CO;2](https://doi.org/10.1130/0091-7613(1984)12<350:FFBEAS>2.0.CO;2).
- Bouquet, A., Sejourne, A., Costard, F., Bouley, S., and Leygueda, E., 2020, Glacial landscape and paleoglaciation in Terra Sabaea: Evidence for a 3.6 Ga polythermal plateau ice cap: Geomorphology, v. 350, <https://doi.org/10.1016/j.geomorph.2019.106858>.
- Brauch, K., Pohl, C., Symons, G., and Tauchnitz, M., 2018, Deliverable D4.2: Paper on Instrument Tests and Best Practice for Carbonatites and Alkaline Rocks: Technical Report, European Union (EU) H2020 HiTech Alk-Carb Project—New Geomodels to Explore Deeper for High-Technology Critical Raw Materials in Alkaline Rocks and Carbonatites, grant agreement no. 689909, 478 p., <https://doi.org/10.13140/RG.2.2.18235.08487>.
- Braunger, S., Marks, M.A.W., Walter, B.F., Neubauer, R., Reich, R., Wenzel, T., Parsapoor, A., and Markl, G., 2018, The petrology of the Kaiserstuhl volcanic complex, SW Germany: The importance of metasomatized and oxidized lithospheric mantle for carbonatite generation: Journal of Petrology, v. 59, p. 1731–1762, <https://doi.org/10.1093/petrology/egy078>.
- Campeny, M., Mangas, J., Melgarejo, J.C., Bambi, A., Alfonso, P., Gernon, T., and Manuel, J., 2014, The Catanda extrusive carbonatites (Kwanza Sul, Angola): An example of explosive carbonatitic volcanism: Bulletin of Volcanology, v. 76, p. 1–15, <https://doi.org/10.1007/s00445-014-0818-6>.
- Capra, L., Macias, J.L., Scott, K.M., Abrams, M., and Garduño-Monroy, V.H., 2002, Debris avalanches and debris flows transformed from collapses in the Trans-Mexican volcanic belt, Mexico—Behavior and implications for hazard assessment: Journal of Volcanology and Geothermal Research, v. 113, p. 81–110, [https://doi.org/10.1016/S0377-0273\(01\)00252-9](https://doi.org/10.1016/S0377-0273(01)00252-9).
- Cas, R.A.F., and Wright, J.V., 1988, Volcanic Successions Modern and Ancient—A Geological Approach to Processes, Products and Successions: London, Chapman and Hall, 528 p., <https://doi.org/10.1007/978-94-009-3167-1>.
- Castro, J.M., and Feisel, Y., 2022, Eruption of ultralow-viscosity basanite magma at Cumbre Vieja, La Palma, Canary Islands: Nature Communications, v. 13, p. 3174, <https://doi.org/10.1038/s41467-022-30905-4>.
- Chen, H., 2000, The geomorphological comparison of two debris flows and their triggering mechanisms: Bulletin of Engineering Geology and the Environment, v. 58, p. 297–308, <https://doi.org/10.1007/s100640000042>.
- Clavero, J., Sparks, R., Huppert, H., and Dade, W., 2002, Geological constraints on the emplacement mechanism of the Paríacota debris avalanche, northern Chile: Bulletin of Volcanology, v. 64, p. 40–54, <https://doi.org/10.1007/s00445-001-0183-0>.
- Cole, P.D., Guest, J.E., Duncan, A.M., and Pacheco, J.-M., 2001, Capelinhos 1957–1958, Faial, Azores: Deposits formed by an emergent Surtseyan eruption: Bulletin of Volcanology, v. 63, p. 204–220, <https://doi.org/10.1007/s004450100136>.
- Comida, P.P., Ross, P.S., Zimanowski, B., Büttner, R., and Dürig, T., 2023, Controls on juvenile ash morphologies in lava fountains: Insights from laboratory experiments: Bulletin of Volcanology, v. 85, p. 23, <https://doi.org/10.1007/s00445-023-01637-0>.
- Cooper, A.F., Gittins, J., and Tuttle, O.F., 1975, The system Na₂CO₃-K₂CO₃-CaCO₃ at 1 kbar and its significance in carbonatite petrogenesis: American Journal of Science, v. 275, p. 534–560, <https://doi.org/10.2475/ajs.275.5.534>.
- Dawson, J.B., Pinkerton, H., Norton, G.E., and Pyle, D.M., 1990, Physicochemical properties of alkali carbonatite lavas: Data from the 1988 eruption of Oldoinyo Lengai, Tanzania: Geology, v. 18, p. 260–263, [https://doi.org/10.1130/0091-7613\(1990\)018<0260:PPOACL>2.3.CO;2](https://doi.org/10.1130/0091-7613(1990)018<0260:PPOACL>2.3.CO;2).
- Deans, T., and Roberts, B., 1984, Carbonatite tuffs and lava clasts of the Tinderet foothills, western Kenya: A study of calcified natrocarbonatites: Journal of the Geological Society, v. 141, p. 563–580, <https://doi.org/10.1144/gsjgs.141.3.0563>.
- Delcamp, A., Delvaux, D., Kwelwa, S., Macheyeki, A., and Kervyn, M., 2016, Sector collapse events at volcanoes in the North Tanzanian divergence zone and their implications for regional tectonics: Geological Society of America Bulletin, v. 128, p. 169–186, <https://doi.org/10.1130/B31119.1>.
- Dèzes, P., Schmid, S.M., and Ziegler, P.A., 2004, Evolution of the European Cenozoic rift system: Interaction of the Alpine and Pyrenean orogens with their foreland lithosphere: Tectonophysics, v. 389, p. 1–33, <https://doi.org/10.1016/j.tectonophysics.2004.06.011>.
- Elliott, H.A.L., Wall, F., Chakhmouradian, A.R., Siegfried, P.R., Dahlgren, S., Weatherley, S., Finch, A.A., Marks, M.A.W., Dowman, E., and Deady, E., 2018, Fenites associated with carbonatite complexes: A review: Ore Geology Reviews, v. 93, p. 38–59, <https://doi.org/10.1016/j.oregeorev.2017.12.003>.
- Fisher, R.V., and Schmincke, H.-U., 1984, Pyroclastic Rocks: Berlin, Springer, 472 p.
- Ghobadi, M., Brey, G.P., Gerdes, A., Höfer, H.E., and Keller, J., 2022, Accessories in Kaiserstuhl carbonatites and related rocks as accurate and faithful recorders of whole rock age and isotopic composition: International Journal of Earth Sciences, v. 111, p. 573–588, <https://doi.org/10.1007/s00531-021-02130-9>.
- Giebel, R.J., Parsapoor, A., Walter, B.F., Braunger, S., Marks, M.A., Wenzel, T., and Markl, G., 2019, Evidence for magma-wall rock interaction in carbonatites from the Kaiserstuhl volcanic complex (southwest Germany): Journal of Petrology, v. 60, p. 1163–1194, <https://doi.org/10.1093/petrology/egz028>.
- Giordano, D., Russell, J.K., and Dingwell, D.B., 2008, Viscosity of magmatic liquids: A model: Earth and Planetary Science Letters, v. 271, p. 123–134, <https://doi.org/10.1016/j.epsl.2008.03.038>.
- Graettinger, A.H., Manville, V., and Briggs, R.M., 2010, Depositional record of historic lahars in the upper Whangaeu Valley, Mt. Ruapehu, New Zealand: Implications for trigger mechanisms, flow dynamics and lahar hazards: Bulletin of Volcanology, v. 72, p. 279–296, <https://doi.org/10.1007/s00445-009-0318-2>.
- Guzmics, T., Berkesi, M., Bodnar, R.J., Fall, A., Bali, E., Milke, R., Vetlányi, E., and Szabó, C., 2019, Natrocarbonatites: A hidden product of three-phase immiscibility: Geology, v. 47, p. 527–530, <https://doi.org/10.1130/G46125.1>.
- Holub, F.V., Rappich, V., Erban, V., Pécskay, Z., Mlčoch, B., and Míková, J., 2010, Petrology and geochemistry of the Tertiary alkaline intrusive rocks at Douřpov, Douřpovské hory volcanic complex (NW Bohemian Massif): Journal of Geosciences (Prague), v. 55, p. 251–278, <https://doi.org/10.3190/jgeosci.074>.
- Hubberten, H.W., Katz-Lehnert, K., and Keller, J., 1988, Carbon and oxygen isotope investigations in carbonatites and related rocks from the Kaiserstuhl, Germany: Chemical Geology, v. 70, p. 257–274, [https://doi.org/10.1016/0009-2541\(88\)90097-6](https://doi.org/10.1016/0009-2541(88)90097-6).
- Ivanov, B.A., and Deutsch, A., 2002, The phase diagram of CaCO₃ in relation to shock compression and decomposition: Physics of the Earth and Planetary Interiors, v. 129, p. 131–143, [https://doi.org/10.1016/S0031-9201\(01\)00268-0](https://doi.org/10.1016/S0031-9201(01)00268-0).

- Jones, A.P., Genge, M., and Carmody, L., 2013, Carbonate melts and carbonatites: Reviews in Mineralogy and Geochemistry, v. 75, p. 289–322, <https://doi.org/10.2138/rmg.2013.75.10>.
- Jones, T.J., Russell, J.K., Brown, R.J., and Hollendonner, L., 2022, Melt stripping and agglutination of pyroclasts during the explosive eruption of low viscosity magmas: Nature Communications, v. 13, p. 992, <https://doi.org/10.1038/s41467-022-28633-w>.
- Karunadasa, K.S., Manoranjan, C.H., Pitawala, H.M.T.G.A., and Rajapakse, R.M.G., 2019, Thermal decomposition of calcium carbonate (calcite polymorph) as examined by in-situ high-temperature X-ray powder diffraction: Journal of Physics and Chemistry of Solids, v. 134, p. 21–28, <https://doi.org/10.1016/j.jpcs.2019.05.023>.
- Katz, K., and Keller, J., 1981, Comb-layering in carbonatite dykes: Nature, v. 294, no. 5839, p. 350–352, <https://doi.org/10.1038/294350a0>.
- Keller, J., 1981, Carbonatitic volcanism in the Kaiserstuhl alkaline complex: Evidence for highly fluid carbonatitic melts at the Earth's surface: Journal of Volcanology and Geothermal Research, v. 9, p. 423–431, [https://doi.org/10.1016/0377-0273\(81\)90048-2](https://doi.org/10.1016/0377-0273(81)90048-2).
- Keller, J., Klaudius, J., Kervyn, M., Ernst, G.G., and Mattsson, H.B., 2010, Fundamental changes in the activity of the natrocarbonatite volcano Oldoinyo Lengai, Tanzania: I. New magma composition during the 2007–2008 explosive eruptions: Bulletin of Volcanology, v. 72, p. 893–912, <https://doi.org/10.1007/s00445-010-0371-x>.
- Kervyn, M., Ernst, G.G., Klaudius, J., Keller, J., Mbende, E., and Jacobs, P., 2008, Remote sensing study of sector collapses and debris avalanche deposits at Oldoinyo Lengai and Kerimasi volcanoes, Tanzania: International Journal of Remote Sensing, v. 29, p. 6565–6595, <https://doi.org/10.1080/01431160802168137>.
- Kervyn, M., Ernst, G.G., Keller, J., Vaughan, R.G., Klaudius, J., Pradal, E., Belton, F., Mattsson, H.B., Mbende, E., and Jacobs, P., 2010, Fundamental changes in the activity of the natrocarbonatite volcano Oldoinyo Lengai, Tanzania: II. Eruptive behaviour during the 2007–2008 explosive eruptions: Bulletin of Volcanology, v. 72, p. 913–931, <https://doi.org/10.1007/s00445-010-0360-0>.
- Kjarsgaard, B.A., de Wit, M., Heaman, L.M., Pearson, D.G., Stiefenhofer, J., Januszcak, N., and Shirey, S.B., 2022, A review of the geology of global diamond mines and deposits: Reviews in Mineralogy and Geochemistry, v. 88, p. 1–117, <https://doi.org/10.2138/rmg.2022.88.01>.
- Kokelaar, B.P., 1983, The mechanism of Surtseyan volcanism: Journal of the Geological Society, v. 140, p. 939–944, <https://doi.org/10.1144/gsjgs.140.6.0939>.
- Kono, Y., Kenney-Benson, C., Hummer, D., Ohfuji, H., Park, C., Shen, G., Wang, Y., Kavner, A., and Manning, C.E., 2014, Ultralow viscosity of carbonate melts at high pressures: Nature Communications, v. 5, p. 5091, <https://doi.org/10.1038/ncomms6091>.
- Kresten, P., and Morogan, V., 1986, Fenitization at the Fen complex, southern Norway: Lithos, v. 19, p. 27–42, [https://doi.org/10.1016/0024-4937\(86\)90013-7](https://doi.org/10.1016/0024-4937(86)90013-7).
- Lorenz, V., and Kurszlauskis, S., 2007, Root zone processes in the phreatomagmatic pipe emplacement model and consequences for the evolution of maar-diatreme volcanoes: Journal of Volcanology and Geothermal Research, v. 159, p. 4–32, <https://doi.org/10.1016/j.jvolgeores.2006.06.019>.
- Liu, S., Fan, H.-R., Yang, K.-F., Hu, F.-F., Rusk, B., Liu, X., Li, X.-C., Yang, Z.-F., Wang, Q.-W., and Wang, K.-Y., 2018, Fenitization in the giant Bayan Obo REE-Nb-Fe deposit: Implication for REE mineralization: Ore Geology Reviews, v. 94, p. 290–309, <https://doi.org/10.1016/j.oregeorev.2018.02.006>.
- Lustrino, M., and Wilson, M., 2007, The circum-Mediterranean anorogenic Cenozoic igneous province: Earth-Science Reviews, v. 81, p. 1–65, <https://doi.org/10.1016/j.earscirev.2006.09.002>.
- Macintyre, R.M., Dawson, J.B., and Mitchell, J.G., 1974, Age of fault movements in the Tanzania sector of the East African Rift system: Nature, v. 247, p. 354–356, <https://doi.org/10.1038/247354a0>.
- McCrea, J.M., 1950, On the isotope chemistry of carbonates and a paleotemperature scale: The Journal of Chemical Physics, v. 18, p. 849–857, <https://doi.org/10.1063/1.1747785>.
- McPhie, J., Doyle, M., and Allen, R., 1993, Volcanic Textures: A Guide to the Interpretation of Textures in Volcanic Rocks: Hobart, Tasmania, Australia, University of Tasmania, Center for Ore Deposits and Exploration Studies, 196 p.
- Míková, J., and Denková, P., 2007, Modified chromatographic separation scheme for Sr and Nd isotope analysis in geological silicate samples: Journal of Geosciences (Prague), v. 52, p. 221–226, <https://doi.org/10.3190/jgeosci.015>.
- Morogan, V., 1989, Mass transfer and REE mobility during fenitization at Alnö, Sweden: Contributions to Mineralogy and Petrology, v. 103, p. 25–34, <https://doi.org/10.1007/BF00371362>.
- Mourão, C., Mata, J., Doucelance, R., Madeira, J., da Silveira, A.B., Silva, L.C., and Moreira, M., 2010, Quaternary extrusive calcio-carbonatite volcanism on Brava Island (Cape Verde): A nepheline-carbonatite immiscibility product: Journal of African Earth Sciences, v. 56, p. 59–74, <https://doi.org/10.1016/j.jafrearsci.2009.06.003>.
- Murtagh, R.M., and White, J.D., 2013, Pyroclast characteristics of a subaqueous to emergent Surtseyan eruption, Black Point volcano, California: Journal of Volcanology and Geothermal Research, v. 267, p. 75–91, <https://doi.org/10.1016/j.jvolgeores.2013.08.015>.
- Németh, K., and Kósik, S., 2020, Review of explosive hydrovolcanism: Geosciences, v. 10, p. 44, <https://doi.org/10.3390/geosciences10020044>.
- Pin, C., Briot, D., Bassin, C., and Poitrasson, F., 1994, Concomitant separation of strontium and samarium-neodymium for isotopic analysis in silicate samples, based on specific extraction chromatography: Analytica Chimica Acta, v. 298, p. 209–217, [https://doi.org/10.1016/0003-2670\(94\)00274-6](https://doi.org/10.1016/0003-2670(94)00274-6).
- Pitcavage, E., Furman, T., Nelson, W.R., Klegga, P.K., and Barifajio, E., 2021, Petrogenesis of primitive lavas from the Toro Ankole and Virunga volcanic provinces: Metasomatic mineralogy beneath East Africa's Western Rift: Lithos, v. 396–397, <https://doi.org/10.1016/j.lithos.2021.106192>.
- Podborodnikov, I.V., Shatskiy, A., Arefiev, A.V., Rashchenko, S.V., Chanyshiev, A.D., and Litasov, K.D., 2018, The system Na₂CO₃-CaCO₃ at 3 GPa: Physics and Chemistry of Minerals, v. 45, p. 773–787, <https://doi.org/10.1007/s00269-018-0961-2>.
- Popov, V.K., Maksimov, S.O., Vrzhosek, A.A., and Chubarov, V.M., 2007, Basaltoid and carbonatite tuffs of Ambinsky volcano (southwestern Primorye): Geology and genesis: Russian Journal of Pacific Geology, v. 1, p. 371–389, <https://doi.org/10.1134/S1819714007040069>.
- Rankin, A., 2005, Carbonatite-associated rare metal deposits: Composition and evolution of ore-forming fluids—The fluid inclusion evidence, in Linnen, R.L., and Samson, I.M., eds., Rare Element Geochemistry and Mineral Deposits: Geological Association of Canada Short Course Notes 17, p. 299–314.
- Rappich, V., Cajz, V., Košťák, M., Pécský, Z., Řídkošil, T., Raška, P., and Radoň, M., 2007, Reconstruction of eroded monogenic Stromboli cones of Miocene age: A case study on character of volcanic activity of the Jicin volcanic field (NE Bohemia) and subsequent erosional rates estimation: Journal of Geosciences (Prague), v. 52, p. 169–180, <https://doi.org/10.3190/jgeosci.011>.
- Rappich, V., Lisec, M., Fiferna, P., and Závada, P., 2017, Application of modern technologies in popularization of the Czech volcanic geoheritage: Geoheritage, v. 9, p. 413–420, <https://doi.org/10.1007/s12371-016-0208-x>.
- Raška, P., and Cajz, V., 2016, Neovolcanic terrain of the České Středohoří Mountains, in Pánek, T., and Hradecký, J., eds., Landscapes and Landforms of the Czech Republic: Cham, Switzerland, Springer, World Geomorphological Landscapes, p. 139–152, https://doi.org/10.1007/978-3-319-27537-6_12.
- Reguir, E.P., Chakhmouradian, A.R., Halden, N.M., Yang, P., and Zaitsev, A.N., 2008, Early magmatic and reaction-induced trends in magnetite from the carbonatites of Kerimasi, Tanzania: Canadian Mineralogist, v. 46, p. 879–900, <https://doi.org/10.3749/canmin.46.4.879>.
- Reid, M.E., 2004, Massive collapse of volcano edifices triggered by hydrothermal pressurization: Geology, v. 32, p. 373–376, <https://doi.org/10.1130/G20300.1>.
- Reid, M.E., Keith, T.E., Kayen, R.E., Iverson, N.R., Iverson, R.M., and Brien, D.L., 2010, Volcano collapse promoted by progressive strength reduction: New data from Mount St. Helens: Bulletin of Volcanology, v. 72, p. 761–766, <https://doi.org/10.1007/s00445-010-0377-4>.
- Rosatelli, G., Wall, F., and Le Bas, M.J., 2003, Potassic glass and calcite carbonatite in lapilli from extrusive carbonatites at Rangwa caldera complex, Kenya: Mineralogical Magazine, v. 67, p. 931–955, <https://doi.org/10.1180/0026461036750152>.
- Rowe, G.L., Jr., 1994, Oxygen, hydrogen, and sulfur isotope systematics of the crater lake system of Poas volcano, Costa Rica: Geochemical Journal, v. 28, p. 263–287, <https://doi.org/10.2343/geochemj.28.263>.
- Schleicher, H., Keller, J., and Kramm, U., 1990, Isotope studies on alkaline volcanics and carbonatites from the Kaiserstuhl, Federal Republic of Germany: Lithos, v. 26, p. 21–35, [https://doi.org/10.1016/0024-4937\(90\)90038-3](https://doi.org/10.1016/0024-4937(90)90038-3).
- Sharma, A., and Tiwari, K.N., 2014, A comparative appraisal of hydrological behavior of SRTM DEM at catchment level: Journal of Hydrology (Amsterdam), v. 519, p. 1394–1404, <https://doi.org/10.1016/j.jhydrol.2014.08.062>.
- Shatskiy, A., Sharygin, I.S., Gavryushkin, P.N., Litasov, K.D., Borzdov, Y.M., Shcherbakova, A.V., Higo, Y., Funakoshi, K.I., Palyanov, Y.N., and Ohtani, E., 2013, The system K₂CO₃-MgCO₃ at 6 GPa and 900–1450°C: The American Mineralogist, v. 98, p. 1593–1603, <https://doi.org/10.2138/am.2013.4407>.
- Sigmund, J., 1996, Diatrembreccien, Mantelxenolithe und Karbonatite in der Kernbohrung KB 2 im Kaiserstuhl [Ph.D. dissertation]: Freiburg, Germany, Albert-Ludwigs-University Freiburg, 154 p.
- Sigmund, J., and Keller, J., 1994, Amphibole and garnet bearing mantle xenoliths in the Kaiserstuhl, Germany: Relation to diatreme and carbonatite: Mineralogical Magazine, v. 58A, p. 840–841, <https://doi.org/10.1180/minmag.1994.58A.2.173>.
- Simonetti, A., and Bell, K., 1994, Nd, Pb and Sr isotopic data from the Napak carbonatite-nepheline centre, eastern Uganda: An example of open-system crystal fractionation: Contributions to Mineralogy and Petrology, v. 115, p. 356–366, <https://doi.org/10.1007/BF00310774>.
- Taylor, H.P., Frechen, J., and Degens, E.T., 1967, Oxygen and carbon isotope studies of carbonatites from the Laacher See District, West Germany, and the Alnö District, Sweden: Geochimica et Cosmochimica Acta, v. 31, p. 407–430, [https://doi.org/10.1016/0016-7037\(67\)90051-8](https://doi.org/10.1016/0016-7037(67)90051-8).
- Tietz, O., and Büchner, J., 2015, The landscape evolution of the Lausitz block since the Palaeozoic—with special emphasis to the neovolcanic edifices in the Lausitz volcanic field (eastern Germany): Zeitschrift der Deutschen Gesellschaft für Geowissenschaften, v. 166, p. 125–147, <https://doi.org/10.1127/zdgg/2015/0031>.
- Ui, T., Takarada, S., and Yoshimoto, M., 2000, Debris avalanches, in Sigurdsson, H., Houghton, B.F., McNutt, S.R., Rymer, H., and Stix, J., eds, Encyclopedia of Volcanoes: San Diego, California, Academic Press, p. 617–626.
- van Wyk de Vries, B., and Delcamp, A., 2015, Volcanic debris avalanches, in Davies, T., and Shroder, J.F., Jr., eds., Landslides Hazards, Risks and Disasters: San Diego, California, Academic Press, p. 131–157, <https://doi.org/10.1016/B978-0-12-396452-6.00005-7>.
- van Wyk de Vries, B., Kerle, N., and Petley, D., 2000, Sector collapse forming at Casita volcano, Nicaragua: Geology, v. 28, p. 167–170, [https://doi.org/10.1130/0091-7613\(2000\)28<167:SCFACV>2.0.CO;2](https://doi.org/10.1130/0091-7613(2000)28<167:SCFACV>2.0.CO;2).
- Varekamp, J.C., and Kreulen, R., 2000, The stable isotope geochemistry of volcanic lakes, with examples from Indonesia: Journal of Volcanology and Geothermal Research, v. 97, p. 309–327, [https://doi.org/10.1016/S0377-0273\(99\)00175-4](https://doi.org/10.1016/S0377-0273(99)00175-4).
- Vasyukova, O., Kostyuk, A., and Williams-Jones, A., 2023, Kovdor to Oldoinyo Lengai—The missing link in car-

- bonatitic magma evolution: *Geology*, v. 51, p. 59–63, <https://doi.org/10.1130/G50672.1>.
- Viladkar, S.G., 2015, Mineralogy and geochemistry of fenitized nephelinites of the Amba Dongar complex, Gujarat: *Journal of the Geological Society of India*, v. 85, p. 87–97, <https://doi.org/10.1007/s12594-015-0196-5>.
- Walter, B.F., Parsapoor, A., Braunger, S., Marks, M.A.W., Wenzel, T., Martin, M., and Markl, G., 2018, Pyrochlore as a monitor for magmatic and hydrothermal processes in carbonatites from the Kaiserstuhl volcanic complex (SW Germany): *Chemical Geology*, v. 498, p. 1–16, <https://doi.org/10.1016/j.chemgeo.2018.08.008>.
- Walter, B.F., Steele-MacInnis, M., Giebel, R.J., Marks, M.A., and Markl, G., 2020, Complex carbonate-sulfate brines in fluid inclusions from carbonatites: Estimating compositions in the system H_2O -Na-K- CO_3 - SO_4 -Cl: *Geochimica et Cosmochimica Acta*, v. 277, p. 224–242, <https://doi.org/10.1016/j.gca.2020.03.030>.
- Walter, B.F., Giebel, R.J., Steele-MacInnis, M., Marks, M.A., Kolb, J., and Markl, G., 2021, Fluids associated with carbonatitic magmatism: A critical review and implications for carbonatite magma ascent: *Earth-Science Reviews*, v. 215, <https://doi.org/10.1016/j.earscirev.2021.103509>.
- Walter, B.F., Giebel, R.J., Siegfried P.R., Gudelius, D., and Kolb, J., 2023, The eruption interface between carbonatitic dykes and diatremes—The Gross Brückaros volcanic field Namibia: *Chemical Geology*, v. 621, <https://doi.org/10.1016/j.chemgeo.2023.121344>.
- Walter, T.R., 2011, Structural architecture of the 1980 Mount St. Helens collapse: An analysis of the Rosenquist photo sequence using digital image correlation: *Geology*, v. 39, p. 767–770, <https://doi.org/10.1130/G32198.1>.
- Wang, L.X., Marks, M.A., Wenzel, T., Von Der Handt, A., Keller, J., Teiber, H., and Markl, G., 2014, Apatites from the Kaiserstuhl volcanic complex, Germany: New constraints on the relationship between carbonatite and associated silicate rocks: *European Journal of Mineralogy*, v. 26, p. 397–414, <https://doi.org/10.1127/0935-1221/2014/0026-2377>.
- Weidendorfer, D., Schmidt, M.W., and Mattsson, H.B., 2017, A common origin of carbonatite magmas: *Geology*, v. 45, p. 507–510, <https://doi.org/10.1130/G38801.1>.
- Weise, A., and Kluge, T., 2020, Isotope exchange rates in dissolved inorganic carbon between 40 °C and 90 °C: *Geochimica et Cosmochimica Acta*, v. 268, p. 56–72, <https://doi.org/10.1016/j.gca.2019.09.032>.
- Weisenberger, T.B., Spürger, S., and Lahaye, Y., 2014, Hydrothermal alteration and zeolitization of the Fohberg phonolite, Kaiserstuhl volcanic complex, Germany: *International Journal of Earth Sciences*, v. 103, p. 2273–2300, <https://doi.org/10.1007/s00531-014-1046-1>.
- Wilson, M., and Downes, H., 2006, Tertiary–Quaternary intra-plate magmatism in Europe and its relationship to mantle dynamics, *in* Gee, D.G., and Stephenson, R.A., eds., *European Lithosphere Dynamics: Geological Society*, London, Memoir 32, p. 147–166, <https://doi.org/10.1144/GSL.MEM.2006.032.01.09>.
- Wimmenauer, W., and Schreiner, A., 2003, *Geologische Karte von Baden-Württemberg—Kaiserstuhl: Freiburg, Germany, Landesamt für Geologie, Rohstoffe und Bergbau Baden-Württemberg*, scale 1:25,000.
- Wolff, J.A., 1994, Physical properties of carbonatite magmas inferred from molten salt data, and application to extraction patterns from carbonatite-silicate magma chambers: *Geological Magazine*, v. 131, p. 145–153, <https://doi.org/10.1017/S0016756800010682>.
- Woolley, A.R., and Church, A.A., 2005, Extrusive carbonatites: A brief review: *Lithos*, v. 85, p. 1–14, <https://doi.org/10.1016/j.lithos.2005.03.018>.
- Woolley, A.R., and Kempe, D.R.C., 1989, Carbonatites: Nomenclature, average chemical compositions, and element distribution, *in* Bell, K., ed., *Carbonatites: Genesis and Evolution*: London, Unwin Hyman, p. 1–14.
- Yanay, N., Wang, Z., Dettmann, D.L., Quade, J., Huntington, K.W., Schauer, A.J., Nelson, D.D., Mc Manus, J.B., Thirumalai, K., Sakai, S., Morillo, A.R., and Mallik, A., 2022, Rapid and precise measurement of carbonate clumped isotopes using laser spectroscopy: *Science Advances*, v. 8, <https://doi.org/10.1126/sciadv.abq0611>.
- Yaxley, G.M., Anenburg, M., Tappe, S., Decree, S., and Guzmics, T., 2022, Carbonatites: Classification, sources, evolution, and emplacement: *Annual Review of Earth and Planetary Sciences*, v. 50, p. 261–293, <https://doi.org/10.1146/annurev-earth-032320-104243>.
- Zimanowski, B., Lorenz, V., and Fröhlich, G., 1986, Experiments on phreatomagmatic explosions with silicate and carbonatitic melts: *Journal of Volcanology and Geothermal Research*, v. 30, p. 149–153, [https://doi.org/10.1016/0377-0273\(86\)90071-5](https://doi.org/10.1016/0377-0273(86)90071-5).
- Zimanowski, B., Büttner, R., Lorenz, V., and Häfele, H.G., 1997, Fragmentation of basaltic melt in the course of explosive volcanism: *Journal of Geophysical Research: Solid Earth*, v. 102, p. 803–814, <https://doi.org/10.1029/96JB02935>.